The Plant Cell, Vol. 31: 2386–2410, October 2019, www.plantcell.org © 2019 ASPB.

The Ectomycorrhizal Fungus *Laccaria bicolor* Produces Lipochitooligosaccharides and Uses the Common Symbiosis Pathway to Colonize *Populus* Roots[OPEN]

Kevin R. Cope,[a,b,1] Adeline Bascaules,[c] Thomas B. Irving,[a,b] Muthusubramanian Venkateshwaran,[b,2] Junko Maeda,[a,b] Kevin Garcia,[a,b,3] Tomás A. Rush,[a,b] Cathleen Ma,[d] Jessy Labbé,[e] Sara Jawdy,[e] Edward Steigerwald,[a] Jonathan Setzke,[a] Emmeline Fung,[a,b] Kimberly G. Schnell,[a,b] Yunqian Wang,[a] Nathaniel Schleif,[a,b] Heike Bücking,[h] Steven H. Strauss,[d] Fabienne Maillet,[f] Patricia Jargeat,[e,g] Guillaume Bécard,[c] Virginie Puech-Pagès,[c] and Jean-Michel Ané[a,b,4]

[a] Department of Bacteriology, University of Wisconsin, Madison, Wisconsin 53706
[b] Department of Agronomy, University of Wisconsin, Madison, Wisconsin 53706
[c] Laboratoire de Recherche en Sciences Végétales, Université de Toulouse, CNRS, UPS, 31326, Castanet-Tolosan, France
[d] Department of Forest Ecosystems and Society, Oregon State University, Corvallis, Oregon 97331
[e] Biosciences Division, Oak Ridge National Laboratory, Oak Ridge, Tennessee 37831
[f] Laboratoire des Interactions Plantes-Microorganismes, Université de Toulouse, INRA, CNRS, 31326, Castanet-Tolosan, France
[g] Laboratoire Evolution et Diversité Biologique, Université de Toulouse, UPS, CNRS, IRD, 31077 Toulouse, France
[h] Department of Biology and Microbiology, South Dakota State University, Brookings, South Dakota 57007

ORCID IDs: 0000-0003-0173-2871 (K.R.C.); 0000-0002-6062-0119 (A.B.); 0000-0003-3040-4543 (T.B.I.); 0000-0001-7023-1988 (M.V.); 0000-0001-5792-9636 (J.M.); 0000-0003-0821-1024 (K.G.); 0000-0002-3207-1466 (T.A.R.); 0000-0002-5387-4719 (C.M.); 0000-0003-0368-2054 (J.L.); 0000-0002-8123-5439 (S.J.); 0000-0001-5134-9497 (E.S.); 0000-0002-2016-7858 (J.S.); 0000-0002-0005-9657 (E.F.); 0000-0002-9261-3028 (K.G.S.); 0000-0002-6252-7233 (Y.W.); 0000-0003-4313-3260 (N.S.); 0000-0002-4040-0944 (H.B.); 0000-0001-9670-3082 (S.H.S.); 0000-0001-6285-4704 (F.M.); 0000-0002-6417-7425 (P.J.); 0000-0002-5085-7577 (G.B.); 0000-0003-4113-7970 (V.P.-P.); 0000-0002-3128-9439 (J.-M.A.)

Mycorrhizal fungi form mutualistic associations with the roots of most land plants and provide them with mineral nutrients from the soil in exchange for fixed carbon derived from photosynthesis. The common symbiosis pathway (CSP) is a conserved molecular signaling pathway in all plants capable of associating with arbuscular mycorrhizal fungi. It is required not only for arbuscular mycorrhizal symbiosis but also for rhizobia–legume and actinorhizal symbioses. Given its role in such diverse symbiotic associations, we hypothesized that the CSP also plays a role in ectomycorrhizal associations. We showed that the ectomycorrhizal fungus *Laccaria bicolor* produces an array of lipochitooligosaccharides (LCOs) that can trigger both root hair branching in legumes and, most importantly, calcium spiking in the host plant *Populus* in a *CASTOR*/*POLLUX*-dependent manner. Nonsulfated LCOs enhanced lateral root development in *Populus* in a calcium/calmodulin-dependent protein kinase (*CCaMK*)-dependent manner, and sulfated LCOs enhanced the colonization of *Populus* by *L. bicolor*. Compared with the wild-type *Populus*, the colonization of *CASTOR*/*POLLUX* and *CCaMK* RNA interference lines by *L. bicolor* was reduced. Our work demonstrates that similar to other root symbioses, *L. bicolor* uses the CSP for the full establishment of its mutualistic association with *Populus*.

INTRODUCTION

Mycorrhizal fungi are filamentous microorganisms that establish symbiotic associations with the roots of ~90% of terrestrial plant species (Brundrett and Tedersoo, 2018). There are four major types of mycorrhizal associations, and the two most ecologically and economically important associations are arbuscular mycorrhizal (AM) and ectomycorrhizal (ECM; van der Heijden et al., 2015; Martin et al., 2016). AM fungi, which belong to the phylum Mucoromycota (subphylum Glomeromycotina; Spatafora et al., 2016, 2017), likely played a crucial role in the successful colonization of land by plants at least 450 million years ago (Remy et al., 1994; Redecker et al., 2000; Heckman et al., 2001; Delaux et al., 2013; Feijen et al., 2018). At present, AM fungi colonize ~72% of plant species, including most agronomically important crops (Brundrett and Tedersoo, 2018). Fossil evidence of ECM associations date back to only 50 million years ago, but molecular clock analyses suggest that they likely evolved at least 130 million years ago (Berbee and Taylor, 1993; Lepage et al., 1997; Wang and Qiu, 2006; Hibbett and Matheny, 2009). ECM fungal species belong to

[1] Current address: Department of Biology and Microbiology, South Dakota State University, Brookings, South Dakota 57007.
[2] Current address: School of Agriculture, University of Wisconsin, Platteville, Wisconsin 53818.
[3] Current address: Department of Crop and Soil Sciences, North Carolina State University, Raleigh, North Carolina 27695.
[4] Address correspondence to jeanmichel.ane@wisc.edu.
The author responsible for distribution of materials integral to the findings presented in this article in accordance with the policy described in the Instructions for Authors (www.plantcell.org) is: Jean-Michel Ané (jeanmichel.ane@wisc.edu).
[OPEN]Articles can be viewed without a subscription.
www.plantcell.org/cgi/doi/10.1105/tpc.18.00676

IN A NUTSHELL

Background: Most land plants form mutually beneficial associations with arbuscular mycorrhizal fungi. These fungi develop specialized nutrient exchange structures called arbuscules within the cells of plant roots. Woody plants, such as trees, can also associate with ectomycorrhizal fungi, which colonize the root surface and develop a network of hyphae known as the Hartig net between plant cells, but not within them. In these associations, the fungus provides the plant with mineral nutrients that it imports from the soil. In return, the plant provides the fungus with fixed carbon derived from photosynthesis. Both types of mycorrhizal associations play essential roles in environmental and agricultural settings. Understanding the molecular mechanisms that regulate their association with plants can help improve crop productivity and agricultural sustainability.

Question: Athough our knowledge of how plants regulate ectomycorrhizal associations is limited, we know much more about arbuscular mycorrhizal associations. Do plants like poplar trees, which associate with both ectomycorrhizal and arbuscular mycorrhizal fungi, use similar signals and signaling pathways to associate with both types of symbionts?

Findings: We discovered that *Laccaria bicolor*, an ectomycorrhizal fungus, produces diffusible signals known as lipochitooligosaccharides, which are similar to those produced by arbuscular mycorrhizal fungi and rhizobial bacteria. In legumes, these molecules are perceived by specific receptors and activate a common symbiosis pathway, which includes bursts of calcium (calcium spiking) within and around plant nuclei. We demonstrated that the diffusible signals produced by *L. bicolor* trigger calcium spiking by activating this signaling pathway in the roots of poplar trees. We also showed that, by decreasing the expression of genes from this pathway, we could affect not only calcium spiking but also the association between poplar and *L. bicolor*, thus demonstrating the relevance of these lipochitooligosaccharides and this signaling pathway in the establishment of ectomycorrhizal associations.

Next steps: Ectomycorrhizal fungi are diverse and colonize many woody plant species. Our goal is to determine which ectomycorrhizal fungi produce lipochitooligosaccharides and whether they use them to colonize their host plants, particularly hosts like pine that lack the components of the common symbiosis pathway and cannot associate with arbuscular mycorrhizal fungi.

one of three fungal phyla, including Ascomycota (subphylum Pezizomycotina), Basidiomycota (subphylum Agaricomycotina), or Mucoromycota (subphylum Mucoromycotina; Spatafora et al., 2017). They associate with 2% of plant species, including mostly woody plants, and they play a crucial role in various forest ecosystems, which cover ~30% of the global terrestrial surface (Tedersoo et al., 2010; Pan et al., 2013).

In both AM and ECM associations, mycorrhizal fungi not only provide their host plant with mineral nutrients mined from the soil, especially phosphorus, nitrogen, and potassium, but also confer protection against a wide range of biotic and abiotic stresses (Jeffries et al., 2003; Smith and Read, 2010; Garcia and Zimmermann, 2014; Garcia et al., 2017). In exchange, the plant delivers to the fungus various forms of photosynthetically derived carbon (Casieri et al., 2013). Although AM and ECM fungi offer similar nutrient exchange services to their host plants, there are distinct differences in the structures they use to do so. AM fungi use hyphopodia as penetration structures to traverse the cell wall of root epidermal cells and enter plant roots where they proliferate both inter- and intracellularly. Ultimately, they form highly branched hyphal structures called arbuscules in root cortical cells. By contrast, ECM fungi form a hyphal sheath or mantle that encases the entire root tip with an underlying network of hyphae called the Hartig net. This network surrounds, but does not penetrate into, plant epidermal and cortical cells (Balestrini and Bonfante, 2014). The arbuscule and Hartig net both provide interfaces for the exchange of nutrients between host and fungus.

Given the crucial role of mycorrhizal associations in both natural and agricultural environments, extensive research has focused on determining their evolutionary origin, the molecular mechanisms regulating their development, and the benefits that they provide to plants (Bonfante and Genre, 2010; Garcia et al., 2015; Strullu-Derrien et al., 2018). Over the past two decades, significant advances have been made in elucidating the molecular signaling mechanisms required for AM fungi to colonize plants (Kamel et al., 2017; Luginbuehl and Oldroyd, 2017; MacLean et al., 2017; Choi et al., 2018). In brief, low phosphorus availability in the soil leads to reduced phosphorus levels within plant tissues (Kafle et al., 2019). This deficiency triggers increased biosynthesis of strigolactones, a class of plant hormones that also function as signaling molecules for AM fungi (Akiyama and Hayashi, 2006; Yoneyama et al., 2007; Gomez-Roldan et al., 2008; Umehara et al., 2008). These strigolactones are exported across the plasma membrane into the rhizosphere by the ATP binding cassette transporter PLEIOTROPIC DRUG RESISTANCE1 (PDR1; Kretzschmar et al., 2012). Upon detection by AM fungi, strigolactones induce spore germination and hyphal branching (Akiyama et al., 2005; Besserer et al., 2006, 2008). Through an unknown signaling mechanism, strigolactones also stimulate AM fungi to produce short-chain (four- to five-chain) chitin oligomers (COs; Genre et al., 2013). Both COs and lipochitooligosaccharides (LCOs; Maillet et al., 2011) are components of the complex Myc factors that AM fungi produce to communicate with the host plant (Sun et al., 2015).

Initially, LCOs were identified as essential signaling molecules produced by most rhizobia (Lerouge et al., 1990). Their discovery was made possible by using a bioassay known as root hair branching, a phenomenon characterized by a transient cessation of polarized root hair growth and the subsequent re-polarization of growth in a different direction, leading to a characteristic root hair deformation (Heidstra et al., 1994). Root hair branching was used

to study the activity of nodulation (Nod) factors produced by rhizobia on the roots of legumes (Bhuvaneswari and Solheim, 1985). The first chemical structure of a Nod factor from *Rhizobium meliloti* was determined by mass spectrometry and was shown to be a sulfated β-1,4-tetrasaccharide of D-glucosamine with three acetylated amino groups and one acylated with a C16 bisunsaturated fatty acid. This purified LCO specifically induced root hair branching at nanomolar concentrations in the host alfalfa (*Medicago sativa*), but not in the nonhost common vetch (*Vicia sativa*; Lerouge et al., 1990). This host-specific induction of root hair branching in alfalfa was conferred by a sulfate group on the reducing end of the LCO (Truchet et al., 1991). Thus, root hair branching is an excellent bioassay for LCO detection because specific leguminous plant species are extremely sensitive to and are only induced by specific LCO structures. The same root hair branching assays with *V. sativa* were later used to detect the presence and activity of nonsulfated LCOs (nsLCOs) purified from germinating spore exudates (GSEs) of the AM fungus *Rhizophagus irregularis*. Mass spectrometry was also used to further characterize the precise LCO structures (Maillet et al., 2011).

During AM symbiosis, both short-chain COs and LCOs are released into the rhizosphere and function as signaling molecules to the plant. They are perceived on the plasma membrane of the host plant by lysine-motif receptor-like kinases that function in concert with a leucine-rich repeat receptor-like kinase coreceptor termed NORK/DMI2/SymRK (Stracke et al., 2002; Op den Camp et al., 2011; Miyata et al., 2014; Zhang et al., 2015). NORK interacts with 3-hydroxy-3-methylglutaryl CoA reductase1 (HMGR1), leading to the production of mevalonate (Kevei et al., 2007; Venkateshwaran et al., 2015). Through an unknown cascade of events, mevalonate activates a suite of both nuclear ion channels (including CASTOR, DMI1/POLLUX) and cyclic nucleotide-gated calcium channels. These ion channels facilitate the flow of calcium ions (Ca^{2+}) from the perinuclear space into both the nucleoplasm and the cytoplasm immediately surrounding the nucleus (Ané et al., 2004; Charpentier et al., 2008, 2016; Venkateshwaran et al., 2012, 2015). A calcium ATPase, MCA8, localized to the nuclear membrane actively pumps Ca^{2+} back into the perinuclear space, thus inducing repetitive oscillations in Ca^{2+} concentration within and around the nucleus (Capoen et al., 2011). This phenomenon is commonly referred to as Ca^{2+} spiking and is dependent on all of the components described above from the lysine-motif receptor-like kinases to the nuclear ion channels. COs and LCOs are capable of triggering Ca^{2+} spiking even in the absence of the fungus (Genre et al., 2013; Sun et al., 2015).

Repetitive Ca^{2+} spikes in the nucleoplasm lead to the activation of the calcium- and calmodulin-dependent protein kinase DMI3/CCaMK that then phosphorylates its primary target, the transcription factor IPD3/CYCLOPS (Lévy et al., 2004; Messinese et al., 2007; Yano et al., 2008; Horváth et al., 2011; Singh and Parniske, 2012). Upon phosphorylation, IPD3/CYCLOPS regulates the expression of multiple transcription factors required for the development of AM symbiosis (Luginbuehl and Oldroyd, 2017; MacLean et al., 2017; Choi et al., 2018). This elaborate molecular signaling pathway is referred to as the common symbiosis pathway (CSP) because all of the described components are required not only for AM symbioses but also for rhizobia–legume and actinorhizal symbioses (Venkateshwaran et al., 2013; Martin et al., 2017).

A significant body of research on signaling mechanisms in ECM associations exists as well (reviewed in Martin et al., 2016). Regarding diffusible signals released by plants, strigolactones do not appear to affect hyphal branching in the ECM fungal species *Laccaria bicolor* and *Paxillus involutus* (Steinkellner et al., 2007). However, the flavonol rutin stimulated hyphal growth in *Pisolithus tinctorius* and the cytokinin zeatin altered hyphal branch angle (Lagrange et al., 2001). Multiple diffusible signals produced by ECM fungi altered plant growth and development: hypaphorine from *Pisolithus tinctorius* inhibited root hair elongation and induced increased cytosolic Ca^{2+} concentration in *Eucalyptus globulus* (Ditengou et al., 2000; Dauphin et al., 2007), auxin released by an overproducing mutant of *Hebeloma cylindrosporum* exhibited increased mycorrhizal activity (Gay et al., 1994), and auxin released by *L. bicolor* enhanced lateral root formation in *Populus* (Felten et al., 2009, 2010; Vayssières et al., 2015). Diffusible signals from AM fungi were also shown to stimulate enhanced lateral root development in *Medicago truncatula* (Oláh et al., 2005). Later, these signals were identified as nsLCOs and sulfated LCOs (sLCOs), and both induced lateral root formation in a CSP-dependent manner (Maillet et al., 2011).

Given the role of the CSP in three distinct beneficial plant–microbe associations—the AM, rhizobia–legume, and actinorhizal symbioses—we hypothesized that ECM fungi produce LCOs to communicate with their host via activation of the CSP. To test this hypothesis, we used the model basidiomycete ECM fungus *L. bicolor* and the host plant *Populus*, a model woody plant species that contains all of the components of the CSP in its genome (Garcia et al., 2015). Here, we present data that confirm our hypothesis using biological, biochemical, and molecular techniques.

RESULTS

Laccaria bicolor Produces LCOs

We chose the ECM fungus *L. bicolor* as part of our experimental system because it is was the first ECM fungus to have its genome sequenced (Martin et al., 2008). It has therefore become the primary model fungus for studying ECM associations. To determine whether LCOs are produced by *L. bicolor*, we first performed root hair branching assays with two species of model legumes, *M. truncatula* and *Vicia sativa*. Use of these two species for bioassays allowed us to screen for both sLCOs and nsLCOs, respectively, in hyphal exudates from *L. bicolor*. In response to the exudates, root hair branching occurred in both *M. truncatula* and *V. sativa* at a level comparable to the level induced by the positive control for each species—sLCOs (10^{-8} M) and nsLCOs (10^{-8} M), respectively. GSEs from *Rhizophagus irregularis* were applied as an additional positive control and also induced root hair branching. We did not observe root hair branching in either plant species in response to mock or tetra-*N*-acetyl chitotetraose (CO4, 10^{-6} M; Figure 1A) treatments. We quantified the amount of root hair branching that occurred in response to each treatment on 3-cm root fragments from five roots of each plant species (Supplemental Figure 1). Our results suggest that *L. bicolor* produces both sLCOs and nsLCOs.

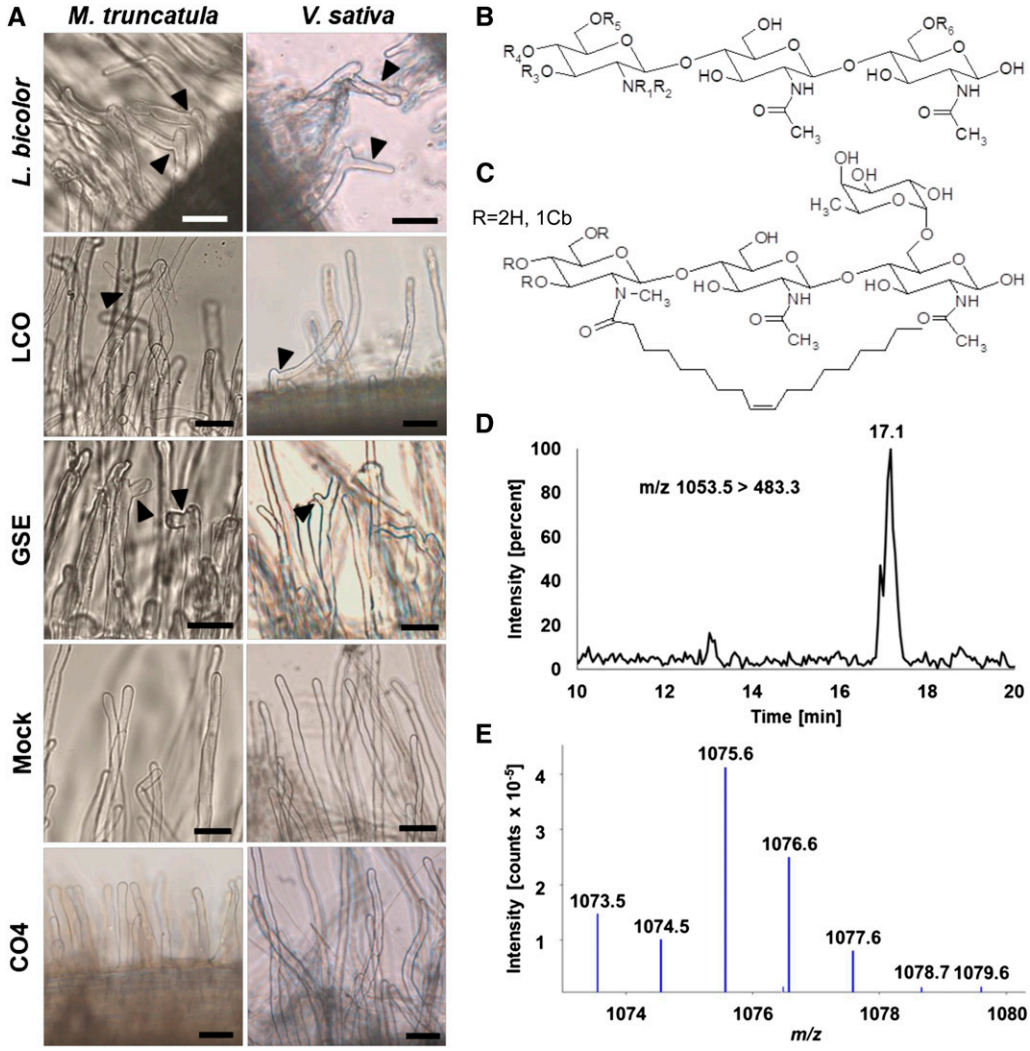

Figure 1. Detection of LCOs Produced by the ECM Fungus *L. bicolor* Using Root Hair Branching Assays and Mass Spectrometry.

(A) Representative images from root hair branching assays with two species of legumes, *M. truncatula* (left) and *V. sativa* (right). In both species, root hair branching (black arrows) occurred in response to the application of hyphal exudates from *L. bicolor*, LCOs, and GSEs from the AM fungus *Rhizophagus irregularis*. No branching occurred in response either to mock treatment (water + 0.005% ethanol) or to the negative control (CO4; 10^{-6} M). sLCOs (10^{-8} M) and nsLCOs (10^{-8} M) served as the positive control for *M. truncatula* and *V. sativa*, respectively (see also Supplemental Figure 1). Bars = 50 μm.

(B) General structure of LCOs detected by mass spectrometry in the culture medium of *L. bicolor*. Among the LCOs detected were short-chain COs of different lengths (n = 1, 2, or 3 corresponding to CO length III, IV, or V, respectively) with different combinations of functional groups (R_1 = H or methyl [Me], R_2 = fatty acid [C16:0, C18:0 or C18:1], $R_{3,\,4,\,5}$ = H or Cb, R_6 = H or deoxyhexose, proposed as Fuc).

(C) Proposed structure of one of the most representative LCO molecules detected: LCO-III C18:1, N-Me, Cb, Fuc, based on known Nod factors (Price et al., 1992). The deoxyhexose on the reducing end of the structure is proposed to be an L-Fuc and the unsaturation of the fatty acid is proposed to be Δ9. Calculated precursor ion $(M+H)^+$ m/z 1053.5, calculated B1 ion $(M+H)^+$ m/z 483.3.

(D) Single reaction monitoring chromatogram obtained in liquid chromatography-tandem mass spectrometry (reverse phase high-performance liquid chromatography-electrospray ionization-triple quadrupole linear ion trap) with detection of the precursor ion $(M+H)^+$ m/z 1053.5 giving, after fragmentation, the product ion B1 m/z 483.3. The observed peak is at a retention time of 17.1 min.

(E) High-resolution liquid chromatography–mass spectrometry (Ultra-High Performance Liquid Chromatography Electrospray Ionisation Q-Exactive) in scanning mode (m/z 350-1900) with detection of the precursor ion $(M+Na)^+$ m/z 1075.5622 (calculated for $C_{48}H_{84}N_4O_{21}Na$ = m/z 1075.5520) (7.64 min). See also Supplemental Figures 2 to 8.

We then used mass spectrometry to confirm the presence of LCOs in the culture medium of *L. bicolor* and to determine their structure. Because previous analyses of LCOs have shown that these molecules are naturally produced in very low concentrations (Maillet et al., 2011; Poinsot et al., 2016), we performed the LCO analysis using the targeted mass spectrometry approach called multiple reaction monitoring (MRM) mode. This mode is highly sensitive but requires the selection of a known LCO structure to search for its possible product ions. In this way, we detected LCOs having various lengths of chitin chains (III, IV,

and V) with several classes of fatty acids (C16:0, C18:0, and C18:1) and multiple functional groups on the nonreducing end (N-methyl [N-Me] and carbamoyl [Cb]) on the reducing end (deoxyhexose, proposed as fucose [Fuc]; Figure 1B; Supplemental Table 1; see also Supplemental Figures 2 to 8). The most abundant LCOs were LCO-IV, C18:1, N-Me and LCO-III, C18:1, N-Me, Cb, Fuc. Because of the low sensitivity of high-resolution mass spectrometry analysis in complex matrices, only LCO-III, C18:1, N-Me, Cb, Fuc was visible in the positive mode, in a sodium adduct $(M+Na)^+$ *m/z* 1075.5622 (calculated for $C_{48}H_{84}N_4O_{21}Na$ = *m/z* 1075.5520; Figures 1C to 1E). We looked for sulfated forms of the major LCOs detected in the samples and found that they were less abundant than the nonsulfated form. For example, sLCO-IV, C18:1, N-Me was approximately half the intensity of nsLCO-IV, C18:1, N-Me (Supplemental Figures 7 and 8). These mass spectrometry data confirm our root hair branching results and demonstrate that the ECM basidiomycete *L. bicolor* produces a wide variety of both sLCOs and nsLCOs.

Both the AM Fungus *Rhizophagus irregularis* and Purified Symbiotic Signals Trigger Ca^{2+} Spiking in *Populus*

Given our finding that *L. bicolor* produces LCOs, we hypothesized that they might function as signaling molecules for communicating with a compatible host plant species such as *Populus*. To test this hypothesis, we first evaluated whether *Populus* could undergo a legume-like root hair branching response in response to both nsLCOs and sLCOs. Although neither signal induced root hair branching in *Populus* (Supplemental Figure 9), this finding was not surprising since, to our knowledge, root hair branching has only been reported for legumes (Lerouge et al., 1990; Heidstra et al., 1994) and actinorhizal plants (Cissoko et al., 2018), which both belong to the nitrogen-fixing clade.

A second diagnostic plant response to LCOs is nuclear Ca^{2+} spiking, which has been observed not only in plants within the nitrogen-fixing clade but also in those outside of it (Sun et al., 2015). Therefore, because all of the CSP genes are conserved in the *Populus* genome (Garcia et al., 2015), we hypothesized that nuclear Ca^{2+} spiking could occur in *Populus*. To test this, we first used *Agrobacterium rhizogenes* to stably transform *Populus* with the coding sequence of both nuclear-localized green genetically encoded Ca^{2+} indicator for optical imaging (G-GECO), a Ca^{2+}-sensitive fluorescent sensor (Zhao et al., 2011), and the *Discosoma* sp. red fluorescent protein (*Ds*Red; Supplemental Figure 10). Given that calcium spiking had not been reported in *Populus* previously, we first evaluated the ability of GSE from the AM fungus *Rhizophagus irregularis* to trigger Ca^{2+} spiking in atrichoblasts of lateral roots from the *Populus* G-GECO line. Atrichoblasts are root epidermal cells that do not develop into root hairs, in contrast to trichoblasts that do produce root hairs. We observed that GSE induced nuclear Ca^{2+} spiking in *Populus* that was comparable to that reported previously for other plant species (Figure 2; Supplemental Movie 1). As expected, no spiking occurred in mock-treated roots (Figure 2; Supplemental Movie 2). These results confirmed that nuclear Ca^{2+} spiking is conserved in *Populus*.

Because GSEs contain a mixture of both short-chain COs and LCOs and both signal types can trigger Ca^{2+} spiking in legumes and nonlegumes even in the absence of the fungus (Maillet et al., 2011; Genre et al., 2013; Sun et al., 2015), we examined which of these symbiotic signals could induce Ca^{2+} spiking in *Populus.* For this experiment, we treated *Populus* roots with nsLCOs, sLCOs, and CO4 and observed that each of the three signals could induce Ca^{2+} spiking (Figures 3A and 3B; Supplemental Movies 3 to 5). To determine whether *Populus* has different sensitivity to these specific signals, we also evaluated the percentage of cells exhibiting Ca^{2+} spiking in response to all three signals at varying concentrations (10^{-10}, 10^{-9}, 10^{-8}, and 10^{-7} M). We observed that only 3% of *Populus* root atrichoblasts exhibited a Ca^{2+} spiking response when treated with nsLCOs at 10^{-10} M. No spiking occurred in response to sLCO and CO4 at the same concentration. However, as the concentration of each signal type increased, so, too, did the number of spiking nuclei. In particular, *Populus* was more sensitive to nsLCOs than sLCOs and CO4 at 10^{-8} M (P-value < 0.05) but equally responsive to all three at 10^{-7} M (Figure 3C). Therefore, at that concentration, we calculated the average number of spikes per nuclei that were induced by each signal type using GSE as a control. We found that the average number of spikes per nucleus was comparable between the nsLCOs and GSE treatments and higher than for the sLCOs and CO4 treatments (P-value < 0.05; Figure 3D). These results indicate that nsLCOs, sLCOs and CO4 can all induce Ca^{2+} spiking in *Populus* but that the required concentration varies with each signal type. Furthermore, they suggest that *Populus* is more sensitive to nsLCOs than the other purified symbiotic signals tested.

Rhizophagus irregularis–Induced Ca^{2+} Spiking in *Populus* Is Dependent on CASTOR/POLLUX

To confirm that Ca^{2+} spiking in *Populus* was dependent on both CASTOR and POLLUX, we used RNA interference (RNAi) to knock down the expression of the genes encoding both proteins. Because *Populus* contains two copies for both *CASTOR* and *POLLUX* due to a recent whole-genome duplication (Tuskan et al., 2006), we designed two RNAi constructs: one targeting both homologs of *CASTOR* and the other targeting both homologs of *POLLUX*. Both RNAi constructs were separately introduced into *Populus* using *Agrobacterium tumefaciens*. We recovered several independent transformation events for *CASTOR* and *POLLUX*. Shoots were regenerated from calli from each of these transformation events and were propagated to establish stably transformed RNAi lines. Six *CASTOR*- and 11 *POLLUX*-RNAi lines survived and were screened via RT-qPCR to determine the degree of gene knockdown (Supplemental Figure 11). Because of high sequence similarity between *CASTOR* and *POLLUX*, we measured the expression of both genes in the top three candidates from both RNAi lines and found that the RNAi construct for *CASTOR* also knocked down the expression of *POLLUX* and vice versa (Supplemental Figure 12). This allowed us to select one RNAi line (*POLLUX* 201) that, compared with the wild-type *Populus*, had an 89% and 80% reduction in the expression of *CASTOR* and *POLLUX*, respectively (Supplemental Figure 13). We subsequently transformed this line with G-GECO. We successfully generated three independent *CASTOR*/*POLLUX*-RNAi G-GECO

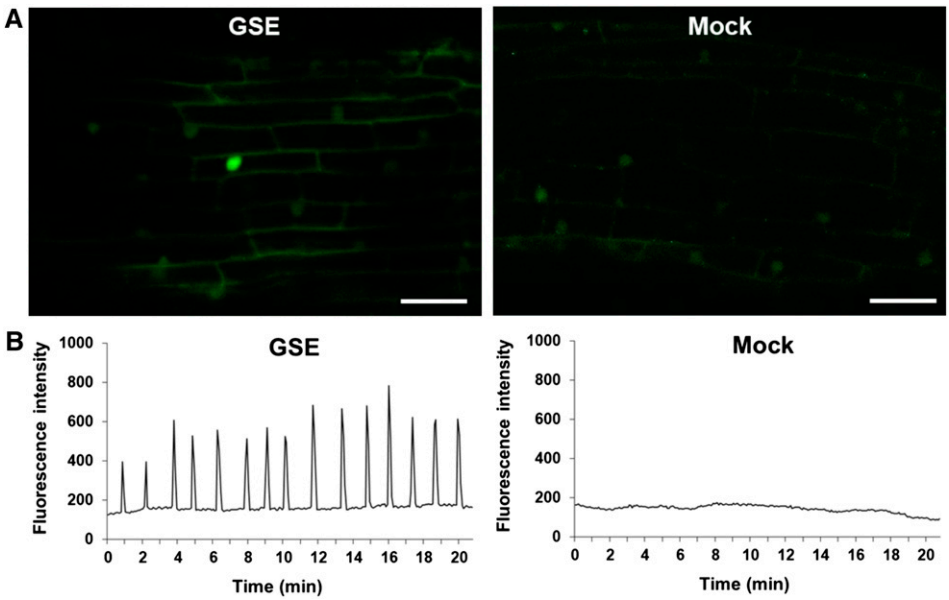

Figure 2. GSEs from the AM Fungus *Rhizophagus Irregularis* Trigger Ca^{2+} Spiking in *Populus*.

(A) Representative confocal images of fluorescing nuclei from atrichoblasts in first-order lateral roots from the *Populus* wild-type G-GECO line (Supplemental Figure 10). GSEs from the AM fungus *Rhizophagus irregularis* (left) induced Ca^{2+} spiking, but mock treatment (right) did not. Note both the elevated fluorescence of the spiking nucleus in the GSE-treated root compared with the basal fluorescence of nonspiking nuclei (see also Supplemental Movie 1) and the absence of elevated fluorescence in nuclei from the mock-treated roots (see also Supplemental Movie 2). Bars = 30 μm.
(B) Plots of Ca^{2+} spiking in *Populus* beginning at ~20 min following application of the same treatments shown in **(A)**. The spiking pattern is representative of that observed in at least three roots with ~20 nuclei per root ($n = 60$ total nuclei). Note the characteristic Ca^{2+} spiking pattern in response to GSE and the absence of Ca^{2+} spiking in mock-treated roots.

lines and used these for our Ca^{2+} spiking assays (Supplemental Figure 14).

We applied GSE onto lateral roots from all three *CASTOR*/*POLLUX*-RNAi G-GECO lines and on the wild-type G-GECO line of *Populus* (Figures 4A and 4B; Supplemental Movies 6 and 7). In all three RNAi G-GECO lines, there was no change in the percentage of spiking nuclei compared with the wild-type G-GECO line (Figure 4C); however, we did see a substantial decrease in the average number of spikes (P-value < 0.001; Figure 4B). Although the spiking intensity appeared to be reduced, we could not measure this directly because G-GECO is not a ratiometric calcium sensor. Nevertheless, our results indicate that the simultaneous RNAi-mediated knockdown of both *CASTOR* and *POLLUX* was sufficient to interfere with their activity and compromise the full activation of the CSP by GSE, and they demonstrate that *CASTOR* and/or *POLLUX* contribute to Ca^{2+} spiking in *Populus.*

The ECM Fungus *L. bicolor* Triggers Ca^{2+} Spiking in *Populus*

To test our hypothesis that *L. bicolor* can trigger Ca^{2+} spiking, we first applied hyphal exudates from *L. bicolor* on first-order lateral roots from the wild-type *Populus* G-GECO line. Although we observed some spiking (Supplemental Movie 8), the response was weak and irregular, perhaps because the concentration of LCOs was low. As such, we repeated the experiment with hyphal fragments of *L. bicolor* in order to place the hyphae in close proximity to the root and potentially elevate the concentration of LCOs. In response to this treatment, Ca^{2+} spiking occurred at a level comparable to the level observed in response to the GSE, while mock treatment did not induce spiking (Figures 5A and 5B; Supplemental Movies 9 to 11). The percentage of spiking nuclei in response to *L. bicolor* hyphae was lower than that in response to GSE from *Rhizophagus irregularis* (P-value < 0.01; Figure 5C); however, the frequency of spiking did not differ between both treatments (Figure 5D). These data show that an ECM fungus is capable of triggering Ca^{2+} spiking comparable to that induced by the AM fungus *Rhizophagus irregularis*.

Given that Ca^{2+} spiking induced by GSE from *Rhizophagus irregularis* was dependent on *CASTOR* and/or *POLLUX*, we hypothesized that Ca^{2+} spiking caused by *L. bicolor* hyphae would be as well. To confirm this, we applied *L. bicolor* hyphae or exudates onto lateral roots from all three *CASTOR*/*POLLUX*-RNAi G-GECO lines and onto the wild-type G-GECO *Populus* as a positive control. Ca^{2+} was not detected in any *CASTOR*/*POLLUX*-RNAi G-GECO roots but was observed in the wild-type G-GECO roots (Figure 6; Supplemental Movies 12 to 14). Based on these results, we concluded that Ca^{2+} spiking in *Populus* induced by *L. bicolor* hyphal fragments is also dependent on *CASTOR* and/or *POLLUX*.

LCOs Affect *Populus* Root Development

Since LCOs from AM fungi enhance lateral root formation in other plant species (Oláh et al., 2005; Gutjahr et al., 2009; Maillet et al., 2011; Mukherjee and Ané, 2011; Sun et al., 2015), we hypothesized

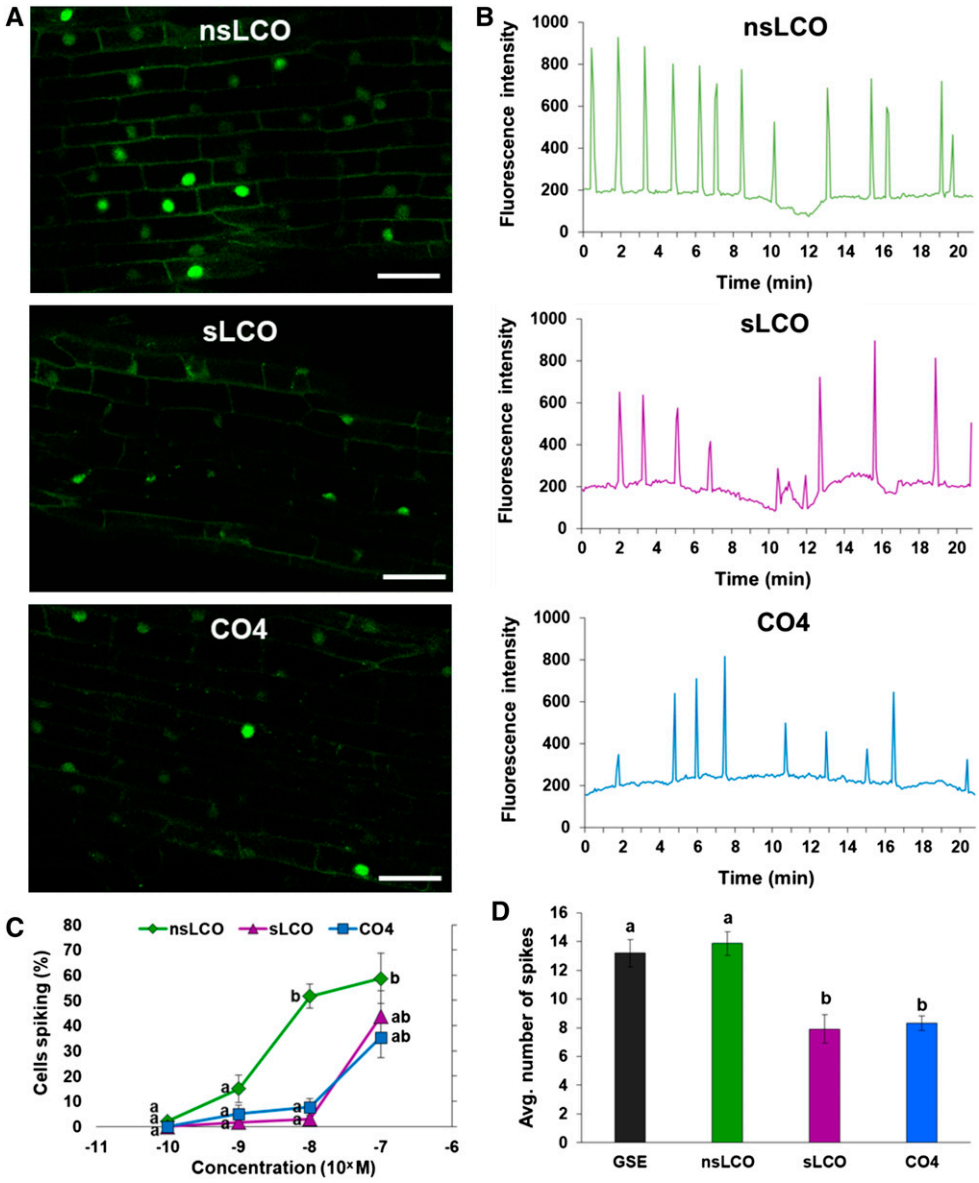

Figure 3. Symbiotic Signaling Molecules Also Cause Ca^{2+} Spiking in *Populus*.

(A) Representative confocal images of fluorescing nuclei from atrichoblasts in first-order lateral roots from the *Populus* wild-type G-GECO line (Supplemental Figure 10) in response to nsLCOs (10^{-7} M; top), sLCOs (10^{-7} M; middle), or CO4 (10^{-6} M; bottom); for all three treatments, note the elevated fluorescence of spiking nuclei compared with the basal fluorescence of nonspiking nuclei (see also Supplemental Movies 3, 4, and 5, respectively). Bars = 30 μm.

(B) Representative plots of Ca^{2+} spiking beginning at ~20 min following application of the same treatments shown in **(A)**.

(C) Percentage of spiking nuclei in *Populus* root atrichoblasts in response to nsLCOs, sLCOs, and CO4 at four concentrations (10^{-10}, 10^{-9}, 10^{-8}, and 10^{-7} M). Data points represent the mean of three roots ($n = 3$ roots) for each treatment at each concentration, and error bars represent the SE of the mean. The data from each treatment type were statistically analyzed by one-way ANOVA (see Supplemental File 1) with Tukey pairwise comparison to assign significance groups (P-value < 0.05). Note the significant increase (P-value < 0.05) in the percentage of cells with spiking nuclei at 10^{-8} M for the nsLCO treatment compared with the other two treatments.

(D) Average spiking frequency of all spiking nuclei from three roots in response to GSE ($n = 59$ spiking nuclei), nsLCOs ($n = 104$), sLCOs ($n = 32$), and CO4 ($n = 92$). Bars represent the mean of the data and error bars represent the SE of the mean. The data were statistically analyzed by one-way ANOVA (see Supplemental File 1) with Tukey pairwise comparison to assign significance groups a and b (P-value < 0.05). Note that the GSE and nsLCO treatments induced significantly higher spiking frequencies compared with the sLCO and CO4 treatments (P-value < 0.05).

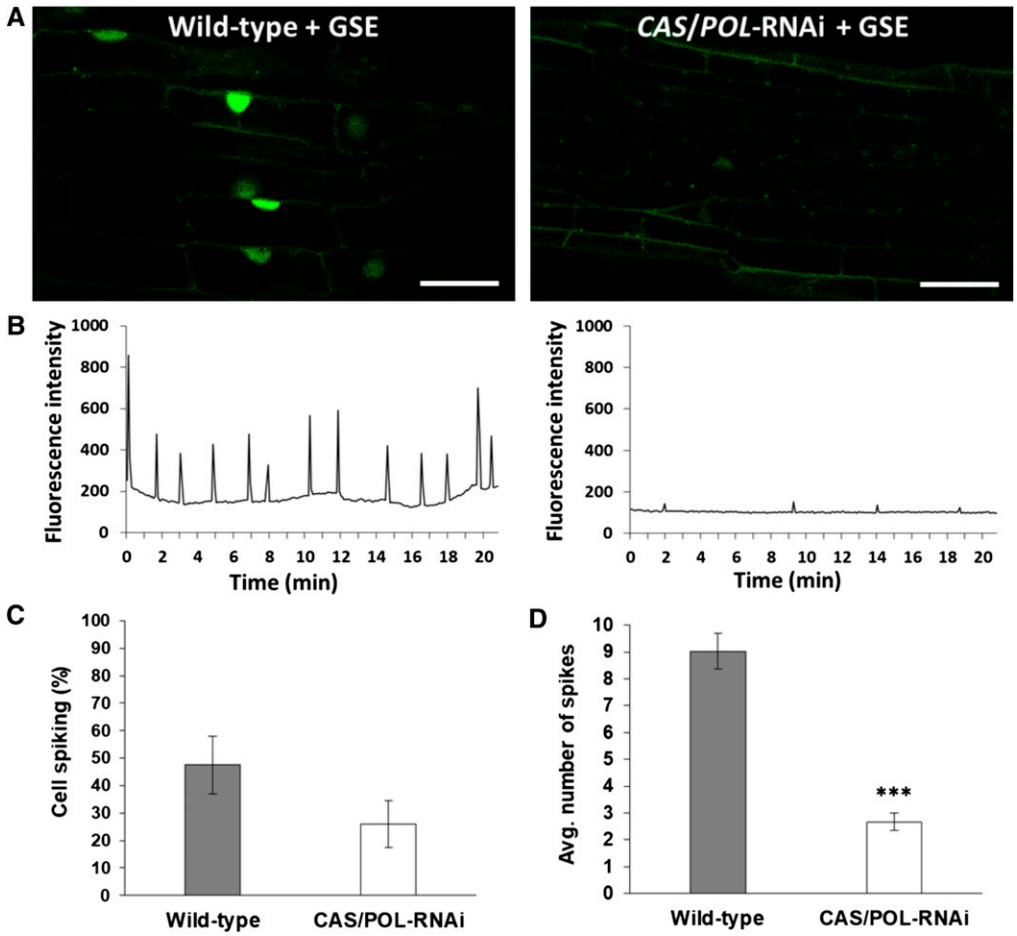

Figure 4. *Rhizophagus Irregularis*–Induced Ca^{2+} Spiking in *Populus* Requires *CASTOR* and *POLLUX*.

(A) Representative confocal images of fluorescing nuclei from atrichoblasts in first-order lateral roots from the *Populus* wild-type G-GECO line (left; see Supplemental Figure 10) and the *CASTOR*/*POLLUX*-RNAi G-GECO line (right; see Supplemental Figure 14), each in response to GSEs from *Rhizophagus irregularis*. Note the elevated fluorescence of the spiking nuclei in the wild-type root compared with the weakly spiking nucleus in the *CASTOR*/*POLLUX*-RNAi root (see also Supplemental Movies 6 and 7, respectively). Bars = 30 μm. *CAS*, *CASTOR*; *POL*, *POLLUX*.

(B) Representative plots of Ca^{2+} spiking in both wild-type and all three *CASTOR*/*POLLUX*-RNAi *Populus* G-GECO lines beginning at ~20 min following application of GSE.

(C) Percentage of spiking nuclei in roots from both *Populus* genotypes (the wild type, $n = 10$ roots and for all three *CASTOR*/*POLLUX*-RNAi lines combined, $n = 13$ roots). The difference between genotypes was not statistically significant (P-value = 0.12). CAS, CASTOR; POL, POLLUX.

(D) Average number of spikes per nucleus for both *Populus* genotypes (the wild type, $n = 77$ nuclei and *CASTOR*/*POLLUX*-RNAi, $n = 45$ nuclei). The difference between genotypes was highly statistically significant (***P-value < 0.001). For both graphs, bars represent the mean of the data and error bars represent the SE of the mean. The data were statistically analyzed by Welch's two-sample *t* test. CAS, CASTOR; POL, POLLUX.

that the previously observed enhancement of lateral root development in *Populus* by *L. bicolor* (Felten et al., 2009) can partially be attributed to the production of LCOs by *L. bicolor*. Furthermore, we hypothesized that if LCOs enhance lateral development in *Populus*, the enhancement would be dependent on the CSP. To test these hypotheses, we used the wild-type *Populus*, the *CASTOR*/*POLLUX*-RNAi line, and a *CCaMK*-RNAi line that we developed with 83% reduction in *CCaMK* expression compared with the wild-type *Populus* line (Supplemental Figures 11 and 13). Before treating all three *Populus* lines with LCOs, we first confirmed that native primary and lateral root development was unchanged in the transgenic RNAi lines compared with the wild type (Figure 7A). Next, we treated all three *Populus* lines with mock, purified nsLCOs, or sLCOs and observed their effect on both primary and lateral root development (Figures 7B and 7C). Primary root length was the same for all of the *Populus* lines regardless of treatment, except for an increase (P-value < 0.05) in the *CASTOR*/*POLLUX*-RNAi line when treated with sLCOs. For lateral root development, in response to nsLCOs, the number of lateral roots per length of primary root increased in both the wild-type and *CASTOR*/*POLLUX*-RNAi lines (P-value < 0.05), whereas the *CCaMK*-RNAi line was nonresponsive to all of the treatments. These data suggest that LCOs affect root development in *Populus* in a CSP-dependent manner and that *L. bicolor* may use nsLCOs as a signal to trigger an increase in lateral root development

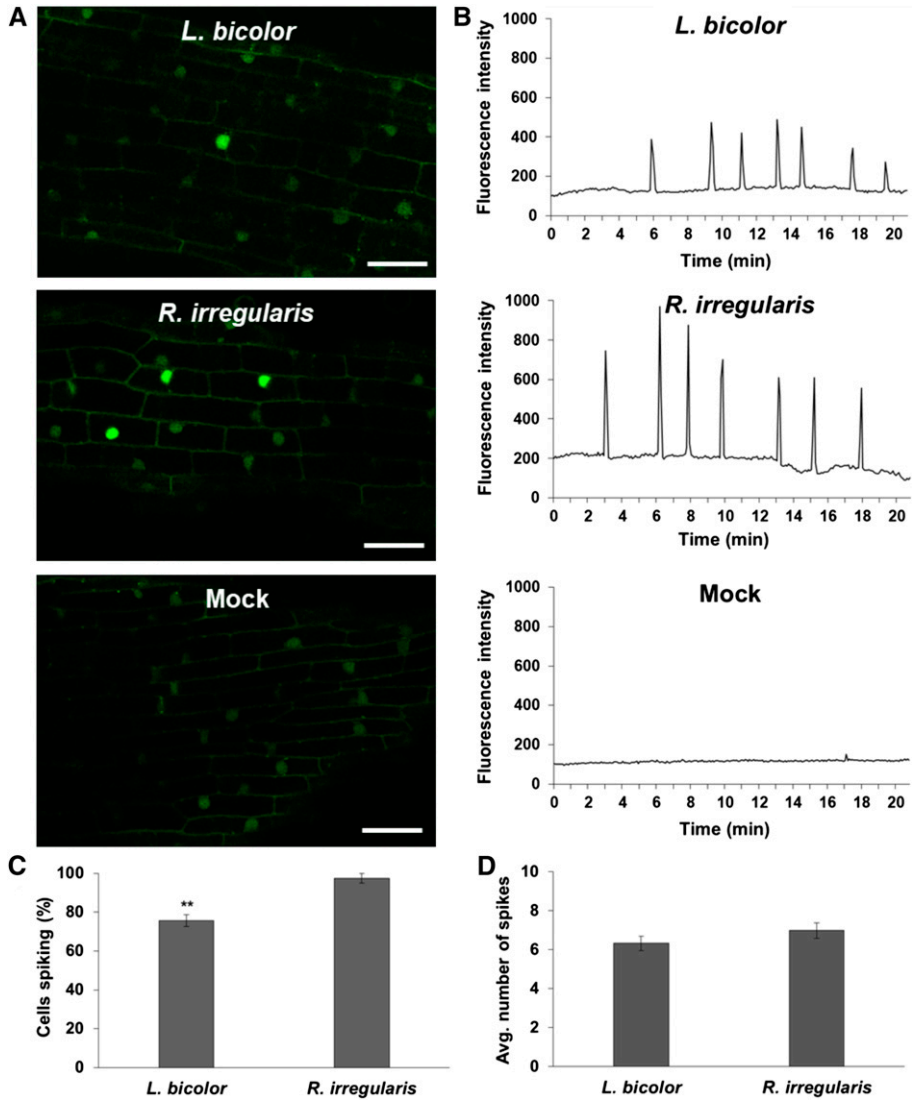

Figure 5. ECM Fungus *L. Bicolor* Triggers Ca^{2+} Spiking in *Populus*.

(A) Representative confocal images of fluorescing nuclei from atrichoblasts in first-order lateral roots from the *Populus* wild-type G-GECO line (Supplemental Figure 10) in response to hyphae from *L. bicolor* (top), GSEs from *Rhizophagus irregularis* (middle), or mock treatment (bottom). Note the elevated fluorescence of spiking nuclei in the *L. bicolor* and *Rhizophagus irregularis* treatments compared with the basal fluorescence of nonspiking nuclei and the absence of spiking nuclei in the mock treatment (see also Supplemental Movies 9, 10, and 11, respectively). Bars = 30 μm.
(B) Representative plots of Ca^{2+} spiking beginning at ~20 min following application of the same treatments shown in **(A)**.
(C) Percentage of spiking nuclei in roots of wild-type *Populus* in response to hyphae from *L. bicolor* ($n = 4$ roots) and GSE from *Rhizophagus irregularis* ($n = 3$ roots). The difference between treatments was statistically significant (**P-value < 0.01).
(D) Average spiking frequency of nuclei from the same roots in response to hyphae from *L. bicolor* ($n = 90$ nuclei) and GSE from *Rhizophagus irregularis* ($n = 65$ nuclei). The difference between treatments was not statistically significant. For both graphs, bars represent the mean of the data and error bars represent the SE of the mean. The data were statistically analyzed by Welch's two-sample *t* test.

independent of *CASTOR/POLLUX* but dependent on *CCaMK*, thereby potentially maximizing root surface area for subsequent colonization.

Application of LCOs Enhances ECM Colonization in *Populus*

After discovering that AM fungi produce LCOs, Maillet et al. (2011) also found that the addition of LCOs significantly enhanced AM colonization in *M. truncatula*. We therefore hypothesized that the application of LCOs could also increase the colonization of *Populus* by *L. bicolor*. To test this hypothesis, we treated established *Populus* roots with purified nsLCOs or sLCOs and subsequently cocultured them with *L. bicolor* using a well-established sandwich system (Felten et al., 2009). As a negative control, we cocultured mock-treated *Populus* roots as well. After 3 weeks of colonization, we harvested the ECM root systems of all treated plants and used

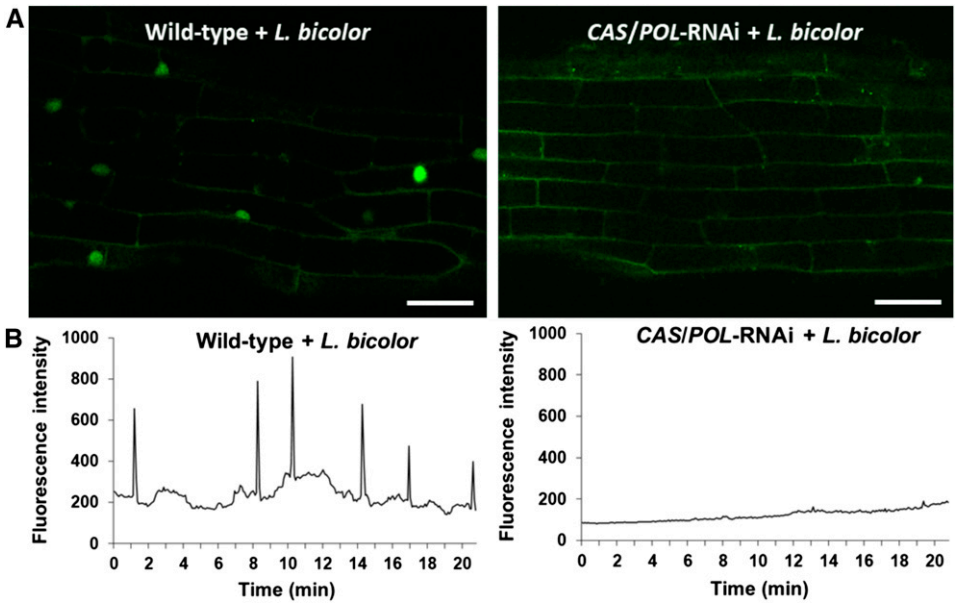

Figure 6. *Laccaria Bicolor*–Induced Ca^{2+} Spiking in *Populus* Requires *CASTOR* and *POLLUX*.

(A) Representative confocal images of fluorescing nuclei from atrichoblasts in first-order lateral roots from the *Populus* wild-type G-GECO line (left; see Supplemental Figure 10) and the *CASTOR*/*POLLUX*-RNAi G-GECO line (right; see Supplemental Figure 14), each in response to hyphal fragments of *L. bicolor*. Note the elevated fluorescence of the spiking nuclei in the wild-type root compared with the absence of spiking nuclei in the *CASTOR*/*POLLUX*-RNAi root (see also Supplemental Movies 12 and 13, respectively). Bars = 30 μm. *CAS*, *CASTOR*; *POL*, *POLLUX*.

(B) Representative plots of Ca^{2+} spiking in both wild-type and all three *CAS*/*POL*-RNAi *Populus* lines beginning at ~20 min following application of hyphal fragments. The spiking pattern is representative of that observed in at least three roots with ~20 nuclei per root (n = 60 nuclei). *CAS*, *CASTOR*; *POL*, *POLLUX*.

a stereomicroscope to observe external mantle formation. However, we did not find any noticeable effect of LCOs (Figure 8A). We also did not see any alteration in primary root length among treatments (Figure 8B), but, as with the previous lateral root experiment, nsLCOs again induced an increase in the number of lateral roots per length of the primary root compared with mock treatment (P value < 0.05; Figure 8C). Surprisingly, this did not result in a significant increase in the number of ECM lateral roots (Figure 8D). Compared with the mock treatment, we saw a decrease (P value < 0.05) in the ratio of ECM lateral roots to the total number of lateral roots in the sLCO treatment (Figure 8E). These results indicate that nsLCOs induce an increase in lateral root formation even in the presence of the fungus.

To identify other potential effects of LCOs, we analyzed in more detail a subset of 20 ECM lateral roots per treatment using confocal microscopy. Using a vibratome, we generated ten 50-μm cross sections from each ectomycorrhiza and then stained the fungal tissue with wheat germ agglutinin conjugated with Alexa Fluor 488 to stain the fungal cell wall and the plant tissue with propidium iodide to stain the plant cell wall (Figure 9A). Following confocal imaging of entire cross sections, we evaluated four parameters: mantle width, root diameter, Hartig net boundary, and root circumference. Based on these measurements, we calculated the ratio of mantle width to root diameter (Figure 9B) and the ratio of Hartig net boundary to root circumference (Figure 9C). Compared with the mock treatment, sLCOs induced a 15 and 8% increase in both ratios, respectively (P-value < 0.05; Figures 9B and 9C). These results suggest that exogenous application of sLCOs, but not nsLCOs, enhances ECM colonization in *Populus*.

Laccaria bicolor Uses the CSP to Colonize *Populus*

Based on our previous data, we hypothesized that *L. bicolor* could use the CSP to colonize *Populus* roots. To test this, we cocultured both the *CASTOR*/*POLLUX*-RNAi and *CCaMK*-RNAi *Populus* lines with *L. bicolor*. We also cocultured the wild-type *Populus* with *L. bicolor* as a control (Figure 10A). After 3 weeks, we harvested, prepared, and observed cross sections of ECM roots (Figure 10B). This allowed us to analyze the same colonization parameters as described for the previous experiment (Figures 10C and 10D). The ratio of mantle width to root diameter in the *CCaMK*-RNAi line decreased by 24% compared with the wild-type *Populus* (P value < 0.05); this decrease did not occur in the *CASTOR*/*POLLUX*-RNAi line (Figure 10C). However, the ratio of Hartig net boundary to root circumference decreased by 15 and 16%, respectively, in the *CASTOR*/*POLLUX*-RNAi and *CCaMK*-RNAi lines compared with the wild type (P value < 0.05; Figure 10D). These results confirmed our hypothesis and clearly illustrate that the ECM fungus *L. bicolor* uses *CCaMK* for the full establishment of the mantle and both *CCaMK* and *CASTOR*/*POLLUX* for Hartig net development during the colonization of *Populus*.

DISCUSSION

Our work demonstrated that the ECM fungus *L. bicolor* produces an array of both nsLCOs and sLCOs (Figure 1). We also showed that *L. bicolor* triggers Ca^{2+} spiking in *Populus* comparable to the

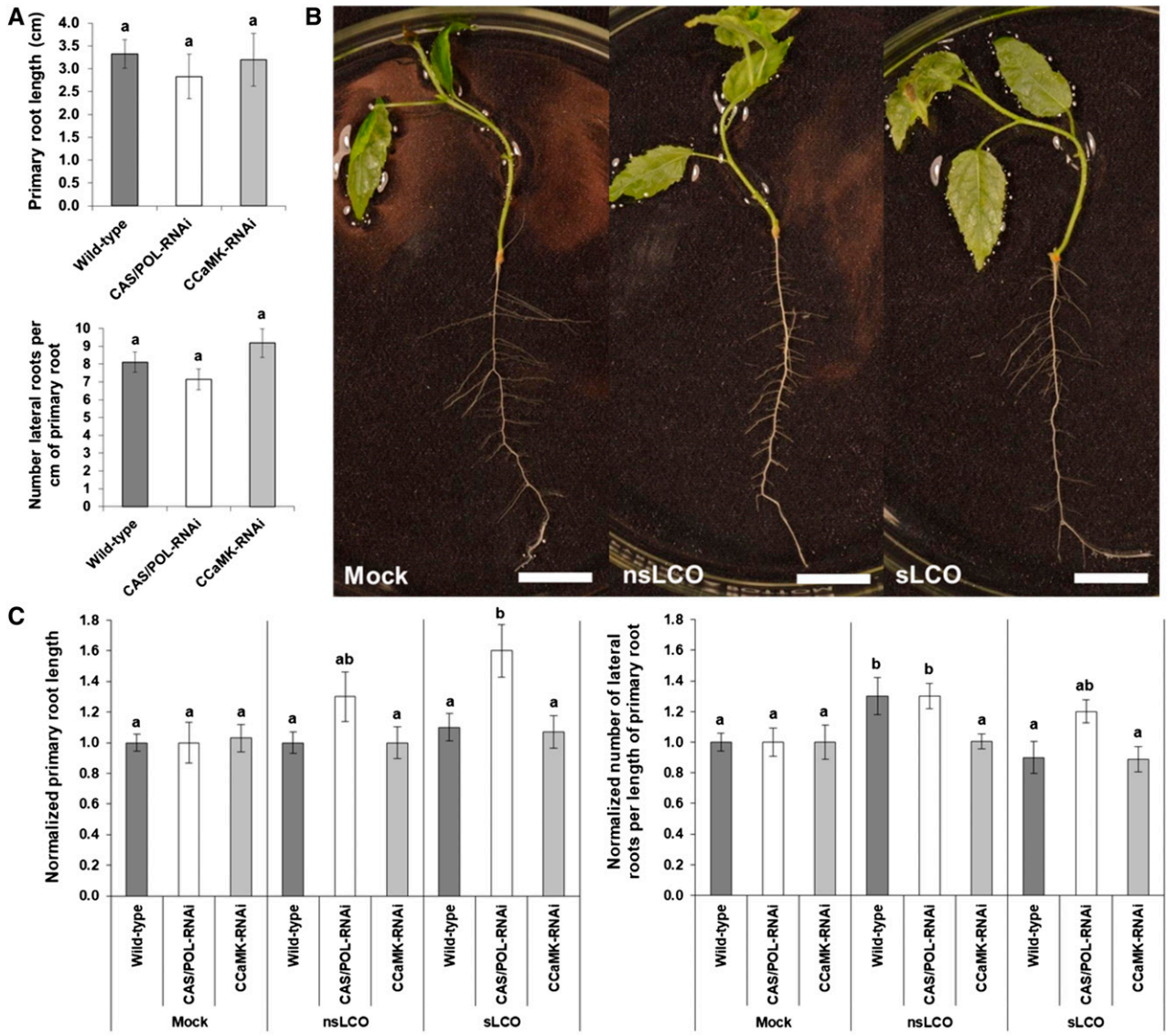

Figure 7. Primary and Lateral Root Development in the Wild-Type, *CASTOR/POLLUX*-RNAi, and *CCaMK*-RNAi *Populus* Lines Treated with LCOs.

(A) Normalized primary root length (top) and normalized number of lateral roots per unit length of primary root (bottom) in the wild-type ($n = 40$ roots), *CASTOR/POLLUX*-RNAi ($n = 38$ roots), and *CCaMK*-RNAi ($n = 38$ roots) *Populus* lines (Supplemental Figure 13). CAS, CASTOR; POL, POLLUX.
(B) Representative images of wild-type *Populus* in response to mock treatment (left), nsLCOs (middle), and sLCOs (right). Bars = 1 cm.
(C) Summary of normalized primary root length (left) and normalized number of lateral roots per length of primary root (right) for the wild-type ($n = 28$, 19, or 16 roots), *CASTOR/POLLUX*-RNAi ($n = 19$, 19, or 16 roots), and *CCaMK*-RNAi ($n = 15$, 16, or 18 roots) *Populus* lines in response to one of three treatments: mock, nsLCOs (10^{-8} M), or sLCOs (10^{-8} M), respectively. For all graphs, bars represent the mean of the data and error bars represent the SE of the mean. The data were statistically analyzed by one-way ANOVA (see Supplemental File 1) with Tukey pairwise comparison to assign significance groups a and b (P-value < 0.05). Note that for primary root length, sLCOs induced an increase in only the *CASTOR/POLLUX*-RNAi line (P-value < 0.05); and for the number of lateral roots per length of primary root, nsLCOs induced an increase in both the wild-type and *CASTOR/POLLUX*-RNAi lines (P-value < 0.05). CAS, CASTOR; POL, POLLUX.

spiking induced by GSE from the AM fungus *Rhizophagus irregularis* (Figures 2 and 5). The Ca^{2+} spiking response in *Populus* to both AM and ECM fungi was dependent on *CASTOR/POLLUX* as has been observed in both legumes and rice (*Oryza sativa*; Figures 4 and 6; Peiter et al., 2007; Charpentier et al., 2008; Chen et al., 2009; Sun et al., 2015). Interestingly, we found that, in terms of Ca^{2+} spiking, *Populus* is more sensitive and responsive to nsLCOs than to either sLCOs or CO4 (Figure 3). Furthermore, nsLCOs enhanced *Populus* lateral root development in a *CCaMK*-dependent manner as observed in *M. truncatula* and rice; but in contrast to *M. truncatula* and rice (Maillet et al., 2011; Sun et al., 2015), the response of *Populus* is *CASTOR/POLLUX*

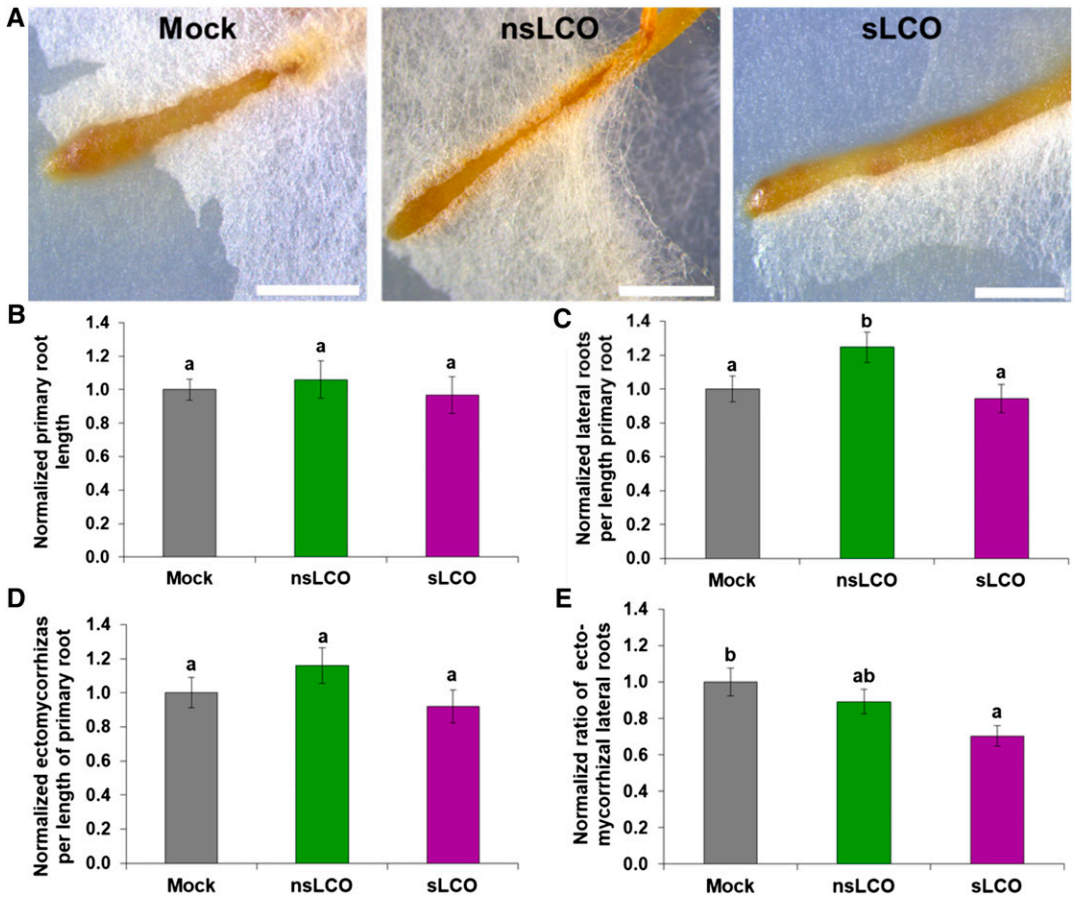

Figure 8. Effect of LCOs on Both Lateral Root and Ectomycorrhiza Formation during *L. Bicolor* Colonization.

(A) Representative stereomicroscope images of the wild-type *Populus* roots treated with mock (left), nsLCOs (10^{-8} M; middle), or sLCOs (10^{-8} M; right) and subsequently cocultured with hyphae of L. *bicolor* for 3 weeks. Bars = 1 mm.

(B) to **(E)** Summary plots of normalized data for root development and ectomycorrhiza formation in response to mock ($n = 17$ roots), nsLCOs ($n = 15$ roots), and sLCOs ($n = 15$ roots), including primary root length **(B)**, number of lateral roots per length of primary root **(C)**, number of ectomycorrhizas per length of primary root **(D)**, and the ratio of ectomycorrhizas per number of lateral roots **(E)**. Note that compared with mock treatment, nsLCOs induced an increase in the number of lateral roots per length of primary root (P-value < 0.05), while sLCOs induced a decrease in the ratio of ectomycorrhizas to total lateral roots (P-value < 0.05). For all graphs, bars represent the mean of the data and error bars represent the SE of the mean. The data were statistically analyzed by one-way ANOVA (see Supplemental File 1) with Tukey pairwise comparison to assign significance groups a and b (P-value < 0.05).

independent (Figure 7). Even in the presence of the fungus, nsLCOs induced an increase in lateral root formation, but this did not result in a significant increase in the ratio of ectomycorrhizas formed (Figure 8). Although the application of sLCOs caused a decrease in the ratio of mycorrhizas developed by *L. bicolor* on *Populus* roots (Figure 8), sLCOs still stimulated a slight increase in mantle and Hartig net formation (Figure 9). Interestingly, the colonization of *M. truncatula* by *Rhizophagus irregularis* was also moderately increased by the application of LCOs (Maillet et al., 2011). Finally, we showed that *L. bicolor* uses *CCaMK* for the full establishment of the mantle and both *CCaMK* and *CASTOR/POLLUX* for complete Hartig net development during the colonization of *Populus* roots (Figure 10). This provides solid evidence that the CSP is used by the ECM fungus *L. bicolor* to colonize its host plant.

Laccaria bicolor Produces a Suite of LCOs with Unique Functions

Although several substitutions on LCOs differ between *Rhizophagus irregularis* and *L. bicolor*, both mycorrhizal fungi produce a mixture of sLCOs and nsLCOs (Maillet et al., 2011). Different structures of LCOs are more active at different steps of the *Populus–L. bicolor* association. Purified nsLCOs induce Ca^{2+} spiking at lower concentrations than sLCOs and enhance lateral root development, while sLCOs did not. Reciprocally, purified sLCOs enhanced ECM colonization, but nsLCOs did not. The roles of different LCO structures at various stages of the symbiotic associations have been well described in the rhizobia–legume symbiosis. For instance, *Sinorhizobium meliloti* produces LCOs O-acetylated and N-acylated by C16-unsaturated fatty acids that are required for infection thread formation and nodule

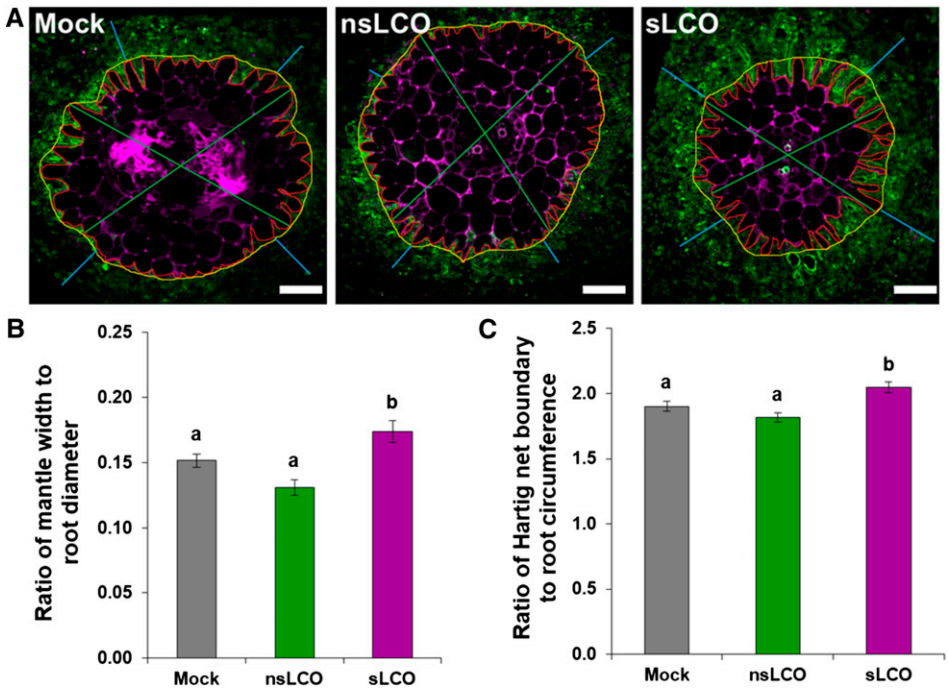

Figure 9. Effect of LCOs on Both Mantle and Hartig Net Formation during *L. bicolor* Colonization.

(A) Representative transverse cross sections of *Populus* roots treated with mock (left), nsLCOs (10^{-8} M; middle), or sLCOs (10^{-8} M; right) and cocultured with *L. bicolor* for 3 weeks. Colonized roots were sectioned and stained with wheat germ agglutinin conjugated with Alexa Fluor 488 (green) and propidium iodide (purple) and imaged on a confocal laser scanning microscope. For each image, four types of measurements were obtained using ImageJ, including mantle width (light blue), root diameter (green), Hartig net boundary (red), and root circumference (yellow). These measurements were used to calculate both the ratio of average mantle width to average root diameter and average Hartig net boundary to average root circumference. Bars = 50 μm.
(B) and **(C)** Summary plots of the ratios of both mantle width to root diameter **(B)** and Hartig net boundary to root circumference **(C)**. These data revealed that sLCOs ($n = 109$ root cross sections), but not nsLCOs ($n = 77$), induced an increase (P-value < 0.05) in ECM colonization compared with the mock treatment ($n = 111$). For both graphs, bars represent the mean of the data and error bars represent the SE of the mean. The data were statistically analyzed by one-way ANOVA (see Supplemental File 1) with Tukey pairwise comparison to assign significance groups a and b (P-value < 0.05). Note that compared with the other two treatments, sLCOs induced a statistically significant increase (P-value < 0.05) in both ratios, indicating an increase ECM colonization.

organogenesis. Double mutants of *nodF* and *nodL* produce LCOs with saturated fatty acids and that lack the *O*-acetyl substitution at the nonreducing end. An *S. meliloti nodF/L* mutant can elicit root hair curling and initiate nodule organogenesis, but it is unable to initiate infection threads. This indicates that different structured LCOs are required for different stages of the symbiotic association. These observations led to the hypothesis that different receptor complexes that recognize different LCO structures may control different steps of the symbiotic association (Ardourel et al., 1995). Given the effect of different LCO structures on lateral root development and ECM colonization, we speculate that in *Populus* different LCO receptor complexes may control lateral root formation and ECM colonization in response to fungal signals. In future studies, it would be interesting to develop *L. bicolor* mutants that produce specific types of LCOs to dissect the role of different LCO receptor complexes at various stages of the ECM association.

Ca^{2+} Spiking Is Conserved in *Populus* and Is Induced by both AM and ECM Fungi

Observing Ca^{2+} spiking in vivo requires the injection of Ca^{2+}-sensitive dyes or the expression of Ca^{2+} sensors (Ehrhardt et al., 1996; Krebs et al., 2012). For the past decade, the most commonly used sensor for observing Ca^{2+} spiking was the Förster resonance energy transfer (FRET)–based yellow cameleon protein YC3.6 or one of its progenitors (Capoen et al., 2011; Krebs et al., 2012; Sun et al., 2015; Venkateshwaran et al., 2015). However, another class of genetically encoded, non–FRET-based, Ca^{2+}-sensitive fluorescent sensors known as GECO were recently developed (Zhao et al., 2011). When compared with FRET-based sensors, based on the signal-to-noise ratio, the dynamic response of GECO is far superior, thus allowing GECO to detect symbiosis-related variations in Ca^{2+} spiking with higher sensitivity (Kelner et al., 2018). As such, we used a nucleus-localized G-GECO to monitor Ca^{2+} spiking in the nuclei of epidermal cells from *Populus* lateral roots treated with symbiotic signals.

Previous studies have reported that Ca^{2+} spiking responses can differ in trichoblasts and atrichoblasts depending on the signal applied (Chabaud et al., 2011; Sun et al., 2015). In this study, we focused our analysis on atrichoblasts because ECM fungi invaginate between epidermal and cortical cells to form the Hartig net. As such, root hairs do not play a direct role during or after the ECM colonization process; in fact, they are suppressed by ECM formation (Nehls, 2008). Nevertheless, while conducting our

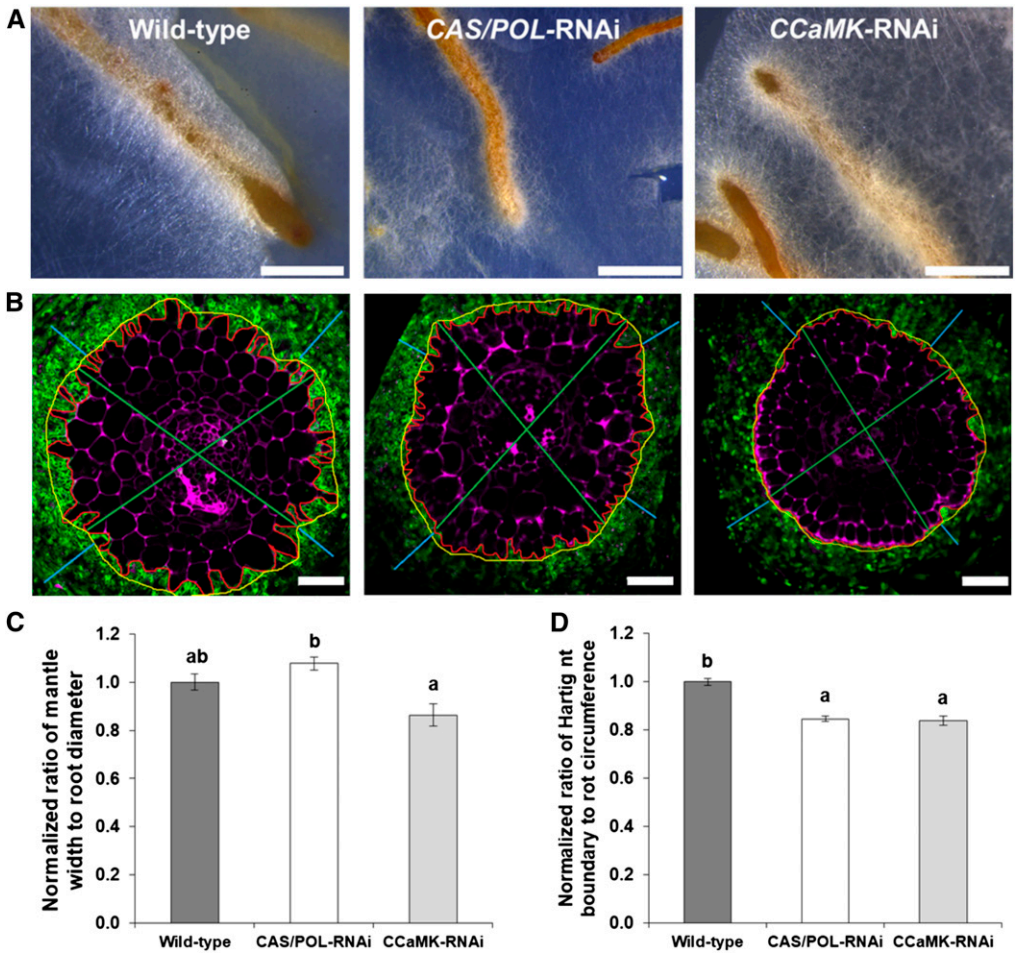

Figure 10. Role of the CSP in the Colonization of *Populus* by the ECM Fungus *L. bicolor*.

(A) Representative stereomicroscope images of the wild-type (left), *CASTOR*/*POLLUX*-RNAi (middle), and *CCaMK*-RNAi *Populus* (right) roots (Supplemental Figure 13) cocultured with *L. bicolor* for 3 weeks. Bars = 1 mm. *CAS*, *CASTOR*; *POL*, *POLLUX*.

(B) Representative transverse cross sections of the wild-type (left), *CASTOR*/*POLLUX*-RNAi (middle), and *CCaMK*-RNAi (right) *Populus* roots cocultured with *L. bicolor*. Colonized roots were sectioned and stained with wheat germ agglutinin conjugated with Alexa Fluor 488 (green) and propidium iodide (purple) and imaged on a confocal laser scanning microscope. For each image, four types of measurements were obtained using ImageJ, including mantle width (light blue), root diameter (green), Hartig net boundary (red), and root circumference (yellow). These measurements were used to calculate both the ratio of average mantle width to average root diameter and average Hartig net boundary to average root circumference. Bars = 50 μm. *CAS*, *CASTOR*; *POL*, *POLLUX*.

(C) and **(D)** Summary plots of the normalized ratios of mantle width to root diameter **(C)** and Hartig net boundary to root circumference **(D)** in the wild-type (n = 240 root cross sections), *CASTOR*/*POLLUX*-RNAi (n = 173), and *CCaMK*-RNAi *Populus* (n = 149) lines. Compared with the wild-type line, both ratios were lower in the *CCaMK*-RNAi line, whereas only the ratio of Hartig net boundary to root circumference was lower in the *CASTOR*/*POLLUX*-RNAi line (P-value < 0.05). For both graphs, bars represent the mean of the data and error bars represent the SE of the mean. The data were statistically analyzed by one-way ANOVA (see Supplemental File 1) with Tukey pairwise comparison to assign significance groups a and b (P-value < 0.05). Note that compared with the wild-type line, both ratios were lower in the *CCaMK*-RNAi line, whereas only the ratio of Hartig net boundary to root circumference was lower in the *CASTOR*/*POLLUX*-RNAi line (P-value < 0.05). CAS, CASTOR; POL, POLLUX.

study, we did observe some Ca^{2+} spiking in the nuclei of trichoblasts (Supplemental Movie 13). Because this was not the focus of our research, we did not pursue this further.

We showed that Ca^{2+} spiking occurs in *Populus* in response to both GSE from the AM fungus *Rhizophagus irregularis* and to purified signals present in GSEs (e.g., LCOs and CO4). Interestingly, we observed that the percentage of spiking nuclei in *Populus* root atrichoblasts was concentration dependent when compared among treatments. Notably, in response to 10^{-8} M nsLCOs, the percentage of spiking nuclei was significantly higher than the response to sLCOs and CO4 at the same concentration. Similarly, the spiking frequency was significantly lower in the CO4 and sLCOs treatments compared with nsLCOs. These two findings suggest that *Populus* is both more sensitive and responsive to nsLCOs. By contrast, nsLCOs and CO4 were less active than sLCOs to initiate Ca^{2+} spiking in lateral roots from *M. truncatula*

(Sun et al., 2015). Also, nsLCOs and CO4 were less active than sLCOs to initiate Ca^{2+} spiking in lateral roots from *M. truncatula* (Sun et al., 2015). In that study, spiking in response to nsLCOs and CO4 was first observed at a concentration of 10^{-8} M with a maximum response at 10^{-6} M, while sLCO spiking began at 10^{-13} M but plateaued at 10^{-9} M. This observation is not surprising given that the LCOs produced by *S. meliloti*—the rhizobial symbiont for *M. truncatula*—are sulfated (Truchet et al., 1991). In contrast to *M. truncatula*, Ca^{2+} spiking in rice occurred primarily in response to CO4, but not at all in response to LCOs (Sun et al., 2015). Combined with these previous finding, our data confirm that different plants respond to and require different signals for the activation of the CSP.

To our knowledge, our work provides the first observation of Ca^{2+} spiking inhibition through RNAi knockdown of *CASTOR* and *POLLUX* as opposed to through the use of mutants. Previous studies with other plant species were based on mutants with complete knockouts of genes required for Ca^{2+} spiking (Charpentier et al., 2008, 2016; Capoen et al., 2011; Sun et al., 2015). At the time we began this study, this was not an option in *Populus* due to the difficulty of obtaining mutant lines. Regardless, we still observed a significant decrease in both spiking frequency and perhaps intensity in response to GSE from *Rhizophagus irregularis*.

In testing the induction of nuclear Ca^{2+} spiking in *Populus* by *L. bicolor*, we first applied the same hyphal exudates as for the root hair branching assays. However, as we observed with the root hair branching assays, the relative concentration of LCOs in the exudates is likely very low and therefore the number of spiking nuclei and spiking frequency were minimal, but still detectable (Supplemental Movie 8). In an attempt to observe an elevated calcium spiking response, we placed *Populus* roots in a suspension of *L. bicolor* hyphal segments that did not inhibit the observation of Ca^{2+} in root atrichoblasts (Supplemental Movies 8, 11, and 12). This technique was the best method for the question we wanted to address and allowed us to observe the expected Ca^{2+} spiking response to LCOs produced by *L. bicolor*; however, there are some limitations to the approach we used. For example, we cannot rule out that the Ca^{2+} spiking we observed was caused by chitin fragments released during the fragmentation of the fungal hyphae. In future studies, a similar system to the one described in Chabaud et al. (2011) could be developed that would allow for the observation of in vivo contact of *Populus* roots with intact *L. bicolor* hyphae. Using this method, one could observe true hyphal-induced Ca^{2+} spiking in *Populus* roots.

LCOs Enhance Lateral Root Development across Species but with Variable Dependence on Components of the CSP

Increased lateral root development is a well-documented response to both AM and ECM fungi (Gutjahr and Paszkowski, 2013; Sukumar et al., 2013; Fusconi, 2014). In response to AM fungal spores from *Gigaspora margarita*, increased lateral root development in *M. truncatula* was dependent on *DMI1/POLLUX* and *SYMRK*, but not *CCaMK* (Oláh et al., 2005). Identical results were obtained with GSE from *Rhizophagus irregularis* (Mukherjee and Ané, 2011). In rice, *Rhizophagus irregularis* induced an increase in lateral root development independent of the CSP (Gutjahr et al., 2009). Again, identical results were observed in response to GSE (Mukherjee and Ané, 2011). However, nsLCOs and sLCOs increased lateral root formation in *M. truncatula*, and this response was entirely dependent not only on *DMI1/POLLUX* and *SYMRK*, but also *CCaMK* (Maillet et al., 2011). Both nsLCOs and sLCOs, as well as CO4, enhanced lateral root formation in rice, and this response to purified signals was dependent on *CCaMK* (Sun et al., 2015). Based on these results, enhanced lateral root formation occurs in both *M. truncatula* and rice in response to AM fungal colonization, application of spores or GSE, and purified signals (COs and LCOs). However, the dependence of these responses on components of the CSP varies by species and by treatment. In our *Populus* experiment, we found that lateral root development was affected by nsLCOs and that this was dependent on *CCaMK*, but not *CASTOR/POLLUX*. Surprisingly, the *CASTOR/POLLUX*-RNAi lines exhibited an enhanced response to LCOs in both primary root length and lateral root development, which were not observed before in other species using mutants.

Interactions between ethylene and auxin are required for lateral root development in multiple plant species (Ivanchenko et al., 2008; Negi et al., 2010). ECM fungi take advantage of this conserved mechanism of hormone balance and manipulate root morphology in various tree species by producing ethylene and auxin (Rupp and Mudge, 1985; Rupp et al., 1989; Karabaghli-Degron et al., 1998; Felten et al., 2009, 2010; Splivallo et al., 2009; Vayssières et al., 2015). Our findings indicate that manipulating hormone balance is not the only mechanism that is used by *L. bicolor* to affect root architecture. Similar to AM fungi (Oláh et al., 2005), *L. bicolor* also produces LCOs to stimulate an increase in lateral root formation and thereby maximizes the root surface area available for colonization.

The CSP Is Likely Not Used for All ECM Associations

AM colonization assays have traditionally been performed with plant mutants to evaluate the role of the core CSP genes in the colonization process (Stracke et al., 2002; Ané et al., 2004; Lévy et al., 2004). Because mutant lines in *Populus* were unavailable when we started this study, the best method for manipulating *Populus* gene expression was RNAi. This method was used previously to knock down the expression of *CCaMK* in tobacco (*Nicotiana attenuata*), resulting in a decrease in AM colonization (Groten et al., 2015). Using RNAi in *Populus*, we generated RNAi lines targeting *CASTOR*, *POLLUX*, and *CCaMK* with 89%, 80%, and 83% knockdown, respectively, compared with the wild-type *Populus*. Because of the time and cost of producing transgenic *Populus*, we did not generate an empty-vector control line but instead used the wild-type poplar since its root development did not differ from the RNAi lines (Figure 7A). Compared with the wild-type, the *CASTOR/POLLUX*- and *CCaMK*-RNAi lines exhibited a decrease in colonization with both the AM fungus *Rhizophagus irregularis* (Supplemental Figure 15) and the ECM fungus *L. bicolor* (Figure 10), further demonstrating that RNAi is a useful tool for evaluating the role of genes involved in plant–microbe interactions. However, the degree of inhibition in the RNAi lines was higher for AM colonization than for ECM colonization, especially in the *CCaMK*-RNAi line. There are multiple explanations for this observation. A previous study of genes involved in AM symbiosis

revealed that high-density inoculum partially overcame the mutant phenotype of multiple CSP genes (Morandi et al., 2005). In our study, we used the well-established sandwich system (Felten et al. , 2009), which allows for the uniform formation of multiple ectomycorrhizas on the same root system. This method of inoculation exposes plant roots to a density of ECM hyphae that exceeds that present in nature. As such, the expected phenotype of reduced colonization may have been somewhat masked by the ability of high-density inoculum to overcome the knock down of the CSP genes partially. Regardless, colonization was reduced in the RNAi lines compared with the wild-type control, thus demonstrating that *L. bicolor* uses the CSP to colonize *Populus.*

Our observation that the CSP plays a role in the establishment of the *Populus–L. bicolor* association is probably not a general rule for all ECM associations. Many genes of the CSP are absent in the genome of pine (*Pinus pinaster*; Garcia et al., 2015), a host plant for the ECM fungus *H. cylindrosporum*. In support of this, the addition of LCOs on roots of *P. pinaster* did not affect lateral root development, suggesting that *P. pinaster* may be incapable of perceiving or responding to LCOs (Supplemental Figure 16). Moreover, the coculture of LCO-treated *P. pinaster* roots with *H. cylindrosporum* did not affect the number of ectomycorrhizas that were formed (Supplemental Figure 17). Because *L. bicolor* produces LCOs and requires the CSP for full colonization of *Populus*, it would be interesting to test whether *L. bicolor* colonization of a host plant that lacks the CSP, for example, Norway spruce (*Picea abies*), is increased with the application of LCOs (Karabaghli-Degron et al., 1998; Garcia et al., 2015). Furthermore, the presence of LCOs in *L. bicolor* raises the question of whether other ECM fungal species also produce LCOs and potentially use them to activate the CSP as part of their mechanisms for plant colonization. The methods described in this article could serve as a platform for future studies in evaluating the presence of LCOs in other species of ECM fungi and evaluating their role during the colonization of compatible host plants.

Some Molecular Mechanisms Required for Individual ECM Associations Are Likely Species Specific

Fossil evidence and molecular studies suggest a single origin for AM symbioses (Brundrett, 2002; Delaux et al., 2014; Bravo et al., 2016). However, phylogenetic studies with ECM fungi suggest that ECM symbioses evolved independently in 78 to 82 fungal lineages (Tedersoo and Smith, 2013; Martin et al., 2016; Hoeksema et al., 2018). It is therefore very likely that the molecular mechanisms required for one ECM fungus to colonize one plant species would differ from those required by the same fungus to colonize another plant species. As evidence of this, in addition to a core regulon, a variable gene regulon was identified in *L. bicolor* during the colonization of two distinct host plants, black cottonwood (*Populus trichocarpa*) and Douglas fir (*Pseudotsuga mensiezii*; Plett et al., 2015). Furthermore, another study that compared the transcriptome of both extraradical mycelium and hyphae derived from mature ectomycorrhizas from 13 ECM fungal species found that some groups of genes based on gene ontology were similarly regulated (Kohler and Mycorrhizal Genomics Initiative Consortium et al., 2015). However, symbiosis-induced genes were mostly restricted to individual species. Even two ECM species of *Laccaria* that diverged ~20 million years ago only shared one-third of *Laccaria* symbiosis-induced orphan genes. This observation suggests that even after the evolution of the ECM lifestyle within a genus, individual species diverged and developed their own set of symbiosis-specific proteins (Kohler and Mycorrhizal Genomics Initiative Consortium et al., 2015; Hoeksema et al., 2018).

It is also likely that host-specific responses may be related to the production of small secreted proteins (SSPs). In *L. bicolor*, two mycorrhiza-induced (Mi)SSPs have been characterized, MiSSP7 and MiSSP8, and both function as effectors in the host plant *Populus* (Plett et al., 2011; Pellegrin et al., 2017). The expression of MiSSP7 is induced by the plant-derived flavonoid rutin and modulates jasmonic acid signaling (Plett and Martin, 2012; Plett et al., 2014). *Populus* also releases SSPs that enter ECM hyphae and alter their growth and morphology (Plett et al., 2017). All of these findings combined with ours provide a complete view of how the *Populus–L. bicolor* association forms. However, a significant amount of research is still necessary to determine how many ECM fungi produce LCOs and whether they use them like *L. bicolor* to colonize their host plants via activation of the CSP. If they do, then the CSP should be considered as more common than previously thought in regulating not only the rhizobia–legume, *Frankia*–actinorhizal, and AM symbioses but also relevant ECM symbioses.

METHODS

Plant Material and Culture

We used seeds from *Medicago truncatula* Jemalong A17 and *Vicia sativa* (L.A. Hearne) for the root hair branching experiments and hybrid *Populus* (*Populus tremula* × *Populus alba* clone INRA 717-1-B4) for all other experiments. The *M. truncatula* seeds were acid scarified for 12 min in full-strength H_2SO_4, sterilized with 8.25% (w/v) sodium hypochlorite, rinsed thoroughly with sterile water, and imbibed for 24 h. Imbibed seeds were placed on 1% agar (Sigma-Aldrich) containing 1 μM gibberellic acid (Sigma-Aldrich) and placed at 4°C for 3 d to synchronize germination. The seeds were then germinated at room temperature (25°C) for up 1 d. The *V. sativa* seeds were surface sterilized with 2.4% (w/v) calcium hypochlorite for 2 min, rinsed three times with sterile water, and then soaked for 4 h. Imbibed seeds were placed on moist germination paper (38 lb, Anchor Paper) on 1% agar (Sigma-Aldrich) containing 1 μM gibberellic acid (Sigma-Aldrich) and placed at 4°C for 7 d to synchronize germination. The seeds were then germinated at room temperature (25°C) for up to 4 d. Fully germinated *M. truncatula* and *V. sativa* seeds were plated on moist germination paper on Fahraeus medium (Fåhraeus, 1957) supplemented with 0.1 μM 2-aminoethoxyvinyl glycine (Sigma-Aldrich). *Populus* plants were maintained in axenic conditions using Lloyd and McCown's woody plant medium (2.48 g L^{-1} basal salts [Caisson Labs] supplemented with 5 mM NH_4NO_3, 2.5 mM $Ca(NO_3)_2 \cdot 4\,H_2O$, 3 μM D-gluconic acid calcium salt, 20 g L^{-1} Suc, pH 5.6, 3.5 g L^{-1} agar, and 1.3 g L^{-1} Gelrite) and grown in glass bottles (6 × 10 cm) sealed with Magenta B-caps (Sigma-Aldrich). Unless indicated otherwise, for all *Populus* experiments, 3-cm terminal cuttings were taken from 4-week-old *Populus* plants and rooted for 1 week in half-strength Murashige and Skoog (MS) medium with vitamins (Caisson Labs) supplemented with 10 μM indole-3-butyric acid (Thermo Fisher Scientific). All plants were grown in a growth chamber (Conviron PGC Flex) set to 25°C with a 16-h day/8-h night photoperiod and ~100 μmol m^{-2} s^{-1} of light provided by fluorescent bulbs (Phillips Silhouette High Output F54T5/841).

Fungal Material and Culture

GSEs from *Rhizophagus irregularis* DAOM 197198 (Premier Tech Biotechnologies) were prepared using ~4000 spores mL^{-1} as described previously by Mukherjee and Ané (2011). The *L. bicolor* strain S238N obtained from Francis Martin (INRA, Nancy, France) was maintained on Pachlewski P05 medium (Müller et al., 2013) with 2% agar (w/v) at 25°C in the dark. For the root hair branching assays, hyphal exudates from *L. bicolor* were obtained as follows: 9 × 9-cm sheets of cellophane were boiled in 1 mM EDTA (Sigma-Aldrich) for 1 h, rinsed three times with milli-Q water, and then autoclaved for 1 h while immersed in water. The cellophane sheets were then placed on Pachlewski P20 medium (Müller et al., 2013) with 2% agar (w/v). Nine 8-mm plugs of *L. bicolor* were placed on the cellophane in positions equidistant from one another. After incubation for ~2 weeks, fungal hyphae covered the surface of the cellophane which was then floated on 30 mL of sterile milli-Q water in a square Petri dish (9 cm × 9 cm) and incubated for 3 d. Hyphal exudates were then collected by pouring off the liquid from multiple plates and concentrating it to 10% of the original volume using a rotary evaporator. The concentrated exudates were then stored at −20°C and thawed as needed for the root hair branching experiments. For Ca^{2+} spiking assays, *L. bicolor* hyphae from liquid cultures grown for 2 months in 50 mL of Pachlewski P05 broth were rinsed with sterile water three times. The hyphae were then resuspended in 20 mL of sterile water and mechanically fragmented for 5 s to generate a liquid suspension of hyphal segments that were immediately applied onto *Populus* roots to induce Ca^{2+} spiking.

Root Hair Branching Assays

We performed an initial screen for root hair branching (Figure 1) and later quantified how frequently root hair branching occurred (Supplemental Figure 1). The methods for these assays differed slightly. For the first screen, hyphal exudates from *L. bicolor* were prepared as described in the "Fungal Material and Culture" section, and then 1 mL of hyphal exudates was applied onto root hairs of *M. truncatula* and *V. sativa* in zone II of developing roots (Heidstra et al., 1994). As positive controls for *M. truncatula* and *V. sativa*, we used sLCOs and nsLCOs, respectively, that were suspended in water with 0.005% ethanol (v/v) at a concentration of 10^{-8} M. We also applied GSE as an additional positive control. Both CO4 and mock—water containing 0.005% ethanol (v/v)—treatments were used as negative controls. After 24 h of horizontal incubation at room temperature on the bench, the treated regions of the roots were screened with an inverted transmission light microscope (Leica DMi1) using a 20×/0.30 Leica PH1 objective. Root hairs on the primary root of at least five plants were observed for each treatment.

Subsequent root hair branching assays (Supplemental Figure 1) were performed slightly differently: *L. bicolor* exudates were extracted from either water or broth cultures of *L. bicolor*. The water cultures were prepared as described in the "Fungal Material and Culture" section for the *L. bicolor* cellophane cultures, except that the fungus was floated on water for 5 d instead of 3 d. The broth cultures were derived from *L. bicolor* grown in 50 mL of liquid modified Melin-Norkrans medium (MMN; PhytoTechnology Laboratories) for 1 month in the dark at room temperature. Both the water and MMN broth were filter sterilized using a low-affinity 0.22-μm polystyrene filter (Corning), and the sterile exudates were stored at room temperature (25°C) in a sterilized glass bottle. The root hair branching activity of both types of exudates was analyzed as follows: 1 mL of sterile exudate was applied onto the roots of 1-week-old *M. truncatula* and *V. sativa* seedlings. Treated plants were incubated at room temperature for 48 h, and the plates in which they were cultured were half covered with aluminum foil to keep the roots in the dark and the leaves in the light. Following incubation, the bottom 3 cm of five roots per treatment ($n = 5$) per plant species were observed. With the exception of GSE, the same positive controls were used as before, and MMN broth was used as an additional negative control.

Production of Hyphal Exudates for Mass Spectrometry

In our previous study of LCOs from *Rhizobium* sp IRBG74, 5 liters of bacterial exudates was not sufficient to detect any LCOs by mass spectrometry (Poinsot et al., 2016). In that study, detection of LCOs was only possible after engineering the strain with extra copies of the regulatory *nodD* gene from *Sinorhizobium* sp NGR234. Similarly, the discovery of LCOs in *Rhizophagus irregularis* was only possible after using 450 liters of sterile culture medium used for AM-colonized carrot (*Daucus carota*) roots and exudates from 40 million germinating AM fungal spores (Maillet et al., 2011). Here, we used a total volume of 6 liters of culture medium from 17 independent cultures of *L. bicolor* (Supplemental Table 1). First, fungal cultures were initiated on modified Pachlewski (MP) medium (Jargeat et al., 2014) overlaid with cellophane membrane with one plug per 55-mm Petri dish or three plugs per 90-mm Petri dish. After 2 to 3 weeks, mycelia were transferred to Petri dishes filled with either liquid MP medium (six independent series) or liquid modified MP medium (2.5 g L^{-1} Glc; 11 independent series). All liquid cultures were incubated at 24°C in the dark for 4 weeks without agitation. The fungal culture media (100 to 400 mL depending on the series) were extracted twice with butanol (1:1, v/v). The pooled butanol phases were washed with distilled water and evaporated under vacuum. The dry extract was re-dissolved in 4 mL of water:acetonitrile (1:1, v/v) and dried under nitrogen.

Mass Spectrometry Analyses

Synthetic lipochitin standards (LCO IV-C16:0, LCO IV-C16:0 S, LCO IV-C18:1, and LCO IV-C18:1 S) obtained from Hugues Driguez (CERMAV) were used to optimize HPLC/QTRAP tandem mass spectrometry detection by MRM, at 10^{-5} M in acetonitrile (ACN):water (1:1, v/v), as described previously by Maillet et al. (2011). For HPLC, the HPLC 3000 (Dionex) was equipped with a C18 reverse-phase column Acclaim 120 (2.1 × 250 mm, 5 μm, Dionex). Separation was achieved using a gradient of ACN/water:acetic acid (1000/1, v/v), started at 30% ACN for 1 min, followed by a 30-min gradient to 100% ACN, followed by an isocratic step at 100% ACN for 5 min, at a constant flow rate of 300 μL min^{-1}. For U-HPLC C18 reverse-phase column C18 Acquity (2.1 × 100 mm, 1.7 μm, Waters) was used. Separation was achieved using a gradient of ACN/water:acetic acid (1000:1, v/v), started at 30% ACN in water for 1 min, followed by an 8-min gradient to 100% ACN, followed by an isocratic step at 100% ACN for 2 min, at a constant flow rate of 450 μL min^{-1}. Ten-microliter samples were injected. The mass spectrometer was a 4500 QTRAP mass spectrometer (Applied Biosystems) with electrospray ionization in the positive ion mode. The samples were analyzed in the MRM and enhanced mass spectrometry–enhanced product ion modes. The capillary voltage was fixed at 4500 V and source temperature at 400°C. Fragmentation was performed by collision-induced dissociation with nitrogen at a collision energy between 22 and 54 V. Declustering potential was between 90 and 130 V and was optimized for each molecule. The MRM channels were set according to the transitions of the proton adduct ion $[M+H]^+$ to the fragment ions corresponding to the loss of one, two, or three *N*-acetyl glucosamine moieties at the reducing end (sulfated or not).

RNAi-Construct Design for Silencing CASTOR, POLLUX, and CCaMK

Because of genome duplication, two homologs of *CASTOR*, *POLLUX*, and *CCaMK* exist in the *Populus* genome (Tuskan et al., 2006): *PtCASTORa* (Potri.019G097000) and *PtCASTORb* (Potri.013G128100), *PtPOLLUXa* (Potri.003G008800) and *PtPOLLUXb* (Potri.004G223400), and *PtCCaMKa*

(Potri.010G247400) and *PtCCaMKb* (Potri.008G011400), respectively. Given that neither copy of these genes had been characterized previously, both copies of each gene were targeted simultaneously for RNA-based gene silencing. For *PtCASTOR*, *PtPOLLUX*, and *PtCCaMK*, respectively, a 175-, 153-, or 200-bp DNA fragment was selected based on sequence similarity between both paralogs of each gene and amplified using compatible primers (Supplemental Table 2). PCR-amplified products were cloned into the pENTR/D-TOPO entry vector following the manufacturer's guidelines (Invitrogen). Subsequently, the *PtCASTORa/b*-RNAi, *PtPOLLUXa/b*-RNAi, and *PtCCaMKa/b*-RNAi fragments were individually cloned into the pK7GWIWG2(II) binary vector using Gateway LR Clonase (Invitrogen; Supplemental Table 3). Following insertion, the resulting RNAi constructs were verified for proper orientation and integrity through sequencing and were introduced into *Agrobacterium tumefaciens* strain AGL1 (Lazo et al., 1991) for transformation into *Populus tremula* × *Populus alba* clone INRA 717-1-B4.

Agrobacterium tumefaciens–mediated *Populus* Transformation

Agrobacterium tumefaciens strain AGL1 was used to transform the RNAi binary vectors into *Populus* as described previously by Filichkin et al. (2006). Briefly, *Agrobacterium* cells harboring the RNAi binary vectors were grown for 24 h in Luria-Bertani broth supplemented with 50 mg L^{-1} rifampicin, 50 mg L^{-1} kanamycin, and 50 mg L^{-1} gentamycin on an orbital shaker at 28°C and 250 rpm. The cells were pelleted by centrifugation at 3500 rpm (1992 RCF) for 30 to 40 min and then resuspended in sufficient *Agrobacterium* induction medium to achieve an OD_{600} of 0.5 to 0.6. Internodal stem segments (3 to 4 mm in length) and leaf discs (4 mm in diameter) were wounded with multiple fine cuts and incubated in the *Agrobacterium* suspension with slow agitation for 1 h. The inoculated explants were cocultivated in callus-induction medium (MS supplemented with 10 μM naphthaleneacetic acid [Sigma-Aldrich]) and 5 μM *N*6-(2-isopentenyl)adenine [Sigma-Aldrich]) at 22°C in darkness for 2 d. Explants were then washed four times in sterile, deionized water and once with wash solution (Han et al., 2000). For selection of transformed calli, explants were transferred to callus-induction medium containing 50 mg L^{-1} kanamycin and 200 mg L^{-1} Timentin (GlaxoSmithKline) for 21 d. Shoots were induced by culturing explants on shoot inducing medium (MS containing 0.2 μM thidizuron [NOR-AM Chemical], 100 mg L^{-1} kanamycin, and 200 mg L^{-1} Timentin [GlaxoSmithKline]) for 2 to 3 months, with subculturing every 3 to 4 weeks. For shoot elongation, explants were transferred onto MS medium containing 0.1 μM 6-benzylaminopurine (Sigma-Aldrich), 100 mg L^{-1} kanamycin, and 200 mg L^{-1} Timentin. The regenerated shoots were rooted on half-strength MS medium supplemented 0.5 μM indole-3-butyric acid (Sigma-Aldrich) and 25 mg L^{-1} kanamycin.

For the *CASTOR*-, *POLLUX*-, and *CCaMK*-RNAi constructs, 259, 303, and 259 independent transgenic events were generated, respectively. After multiple rounds of initial selection based on resistance to kanamycin in the selection medium, 21, 32, and 82 events of *PtCASTOR*-, *POLLUX*-, and *CCaMK*-RNAi, respectively, were further confirmed for the presence of the transgene (RNAi cassette) in the transgenic plants using primers designed on the *Cauliflower mosaic virus* 35S promoter, terminator, and RNAi intron flanking the RNAi fragments (Supplemental Table 3). All of the transgenic RNAi lines were maintained as described in the "Plant Material and Culture" section for further validation of the effect of RNAi-based gene silencing.

RNA Extraction, cDNA Synthesis, and qRT-PCR

RNA was extracted from ~100 mg of root tissue from at least three separate plants for each RNAi line by flash freezing them in liquid nitrogen and pulverizing them with two glass beads using a mixer mill (model MM 400, Retsch). Immediately after, 500 μL of RNA extraction buffer (4 M guanidine thiocyanate, 0.2 M sodium acetate, pH 5.0, 25 mM EDTA, 2.5% polyvinylpyrrolidone [v/v], 2% sarkosyl [v/v], and 1% β-mercaptoethanol [v/v] added just before use) was added to the pulverized root tissue and vortexed for 5 s. Next, 500 μL of 24:1 chloroform:isoamyl alcohol (v/v) was added to the solution and again vortexed for 5 s. Following a 10-min centrifugation at 11,000 rpm and 4°C, 450 μL of the aqueous phase of the solution was placed on a shearing column from the Epoch GenCatch plant RNA purification kit. From this point forward, the manufacturer's protocol was strictly followed. Following the extraction, RNA quantity and quality were evaluated with a Nanodrop spectrophotometer (model ND100, Thermo Fisher Scientific) and suitable RNA was stored at −80°C. Contaminating DNA was removed from RNA samples using the TURBO DNA-*free* kit (Invitrogen) and by following the manufacturer's protocol. RNA quantity and quality were again determined with a Nanodrop spectrophotometer.

To prepare the RNA to serve as a template for cDNA synthesis, 1 μg of RNA in 11.5 μL of RNase-free water was incubated at 65°C with 1 μL of oligo$(dT)_{17}$ for 5 min and then placed on ice for another 5 min. To this solution, the following components were then added: 2 μL of 10 mM dNTP, 4 μL of 5× RevertAid Reverse Transcriptase buffer, 0.5 μL of RiboLock RNase inhibitor, and 1 μL of RevertAid reverse transcriptase (Thermo Fisher Scientific). After incubating for 1 h at 42°C, the transcriptase was inactivated at 70°C for 15 min, and the resulting cDNA was stored at −20°C. RT-qPCR was performed using the Bio-Rad CFX96 real-time PCR system with the CFX Manager v3.0 software (Bio-Rad). Reactions were performed in 96-well plates using SsoAdvanced Universal SYBR Green Supermix (Bio-Rad), 10 nM of each gene-specific primer (Supplemental Table 3), and 1:20 (v/v) cDNA:water. PCR cycling conditions were as follows: 95°C for 3 min, followed by 40 cycles at 95°C for 10 s, 58°C for 25 s, and 72°C for 30 s. The specificity and efficiency of primer pairs were confirmed by analysis of dissociation curves (65 to 95°C) and serial dilution, respectively. Results were expressed as a threshold cycle value. At least three technical replicates and three biological replicates were performed for each sample, and their threshold cycle values were averaged. The standard curve method was used to analyze gene expression in each sample as described previously by El Yahyaoui et al. (2004). Ubiquitin- and putative protein-encoding genes were both used as reference genes as described previously by Felten et al. (2009).

Agrobacterium rhizogenes–Mediated *Populus* Transformation

The *A. rhizogenes* strain ARqua1 was transformed by electroporation with the binary vector pEC11579 provided by Dr. Giles Oldroyd (University of Cambridge, UK). This vector encodes both a nucleus-localized version of the G-GECO calcium sensor and the fluorescent protein DsRed. G-GECO expression was driven by the short 35S promoter derived from the cauliflower mosaic virus, and DsRed expression was driven by the Arabidopsis (*Arabidopsis thaliana*) *UBIQUITIN10* promoter. *Agrobacterium rhizogenes* successfully transformed with pEC11579 was used to generate transgenic *Populus* hairy roots using a slightly modified method described by Yoshida et al. (2015). In brief, leaves from axenic cultures of hybrid *Populus* were wounded with a scalpel by making multiple perpendicular incisions 1 mm in length along the central vein on the abaxial surface of the leaf. Wounded leaves were inoculated for only 5 min on an inversion table with a liquid suspension of transformed *A. rhizogenes* strain ARqua1 that was diluted to an OD_{600} of 0.8 using induction broth. Inoculated leaves were placed on coculture medium for 2 d and then transferred to antibiotic medium containing 200 mg mL^{-1} cefotaxime and 300 mg mL^{-1} Timentin. After ~2 weeks of incubation in the dark at 25°C, transgenic roots appeared from wounded sites (Supplemental Figure 10A). These roots were screened using a fluorescent stereomicroscope (Leica M165 FC), and those visibly expressing DsRed were excised and placed on antibiotic medium containing 15 μM *trans*-zeatin (Cayman Chemical) to induce shoot formation as described previously (Son and Hall, 1990). Shoots appeared within as little as 2 months and were again screened using the same fluorescent

stereomicroscope (Supplemental Figures 10B and 14). Shoots expressing DsRed were excised from the roots and placed in half-strength MS medium that was supplemented with 10 μM indole-3-butyric acid and 5 g L^{-1} of Gelrite (DOT Scientific). The resulting stable transgenic lines were maintained as described in the "Plant Material and Culture" section and used for Ca^{2+} spiking experiments.

Ca^{2+} Spiking Experiments

Because lateral roots of *M. truncatula* are generally more responsive to LCOs than primary roots (Sun et al., 2015), we used first-order lateral roots from *Populus* for our experiments. Primary roots from axenic *Populus* with many lateral roots that were at least 1 cm long were extracted from solid woody plant medium. The lateral roots were individually excised from the primary root and placed in woody plant medium broth with reduced phosphorus (2.5 μM KH_2PO_4) and diminished nitrogen (no NH_4NO_3). To inhibit ethylene production, 0.1 μM 2-aminoethoxyvinyl Gly was added to the broth. After at least 2 h of incubation, lateral roots were removed from the broth, placed on a cover slip (48 × 60 mm), and held in place with high vacuum grease (Dow Corning) which was also used to form a square well around the root. Experimental treatments included the following: GSE, nsLCOs (10^{-7} M), sLCOs (10^{-7} M), CO4 (10^{-6} M; IsoSep), a liquid suspension of *L. bicolor* hyphae, or mock treatment (water with 0.005% ethanol). Approximately 200 μL of each treatment was applied individually onto separate lateral roots expressing G-GECO to evaluate their ability to induce Ca^{2+} spiking in root epidermal cells. After application of the treatment solution, lateral roots were overlaid with an additional cover slip (22 × 40 mm) and incubated for ~20 min. Following the incubation, Ca^{2+} spiking was observed for ~20 min using an LSM780 confocal laser scanning microscope (Carl Zeiss) with an LD C-Apochromat 40×/1.1-W Korr M27 objective. G-GECO was excited with the 488-nm line of an argon laser, and green fluorescent protein (490 to 535 nm) emission was detected using a 488-nm primary dichroic mirror. DsRed was excited with the 561-nm line of an argon laser, and red fluorescent protein (579 to 624 nm) emission was detected using a 561-nm primary dichroic mirror. The images were acquired at 5-s intervals with a scanning resolution of 512 × 512 pixels. Settings (laser intensity, gain, offset, magnification, airy units) were similar between observations for all samples. Following the capture of each ~20-min time-course experiment, spiking nuclei were designated as specific regions of interest using the ZEN software (version 2.3 SP1), and the fluorescence intensity of G-GECO was recorded for each region of interest. For all of the Ca^{2+} spiking experiments (Figures 2 to 3456), the total number of cells with visible nuclei and the number of nuclei spiking more than once were used to calculate the percentage of cells with spiking nuclei. Furthermore, the fluorescence intensity of G-GECO was plotted for each spiking nucleus to determine the frequency of Ca^{2+} spiking events.

Lateral Root and Colonization Assays with *L. bicolor*

Rooted *Populus* cuttings were plated on P20 medium in square Petri dishes (9 × 9 cm) sandwiched between two triangular pieces of cellophane. Plated cuttings were then placed in the growth chamber. For the native lateral root experiments with the wild-type and RNAi *Populus* lines (Figure 7A), no treatment was performed, and the plants were grown for a total of 3 weeks. However, for the LCO-treated experiments (Figures 7B and 7C), the adventitious root system of each plant was trimmed after ~1 week so that only one root remained. It was then immersed for 1 h in mock treatment (water + 0.005% ethanol [v/v]), nsLCOs (10^{-8} M), or sLCOs (10^{-8} M). Treated plants were then plated on fresh Pachlewski P20 medium with cellophane and grown for an additional 2 weeks. At harvest, the number of lateral roots per primary root was counted manually, and the root system was photographed on each side with a D3200 DSLR camera (Nikon). Both images of the root system were analyzed using ImageJ (https://imagej.nih.gov/ij/) to determine the average primary root length. This number was also used to calculate the number of lateral roots per length of primary root.

For the colonization assays, *L. bicolor* was grown for 10 d on triangular sheets of cellophane placed on Pachlewski P20 medium in square Petri dishes (9 × 9 cm) with seven equally spaced 8-mm plugs per sheet and two sheets per dish. After the plugs were removed, the cellophane sheet was placed on fresh Pachlewski P20 medium. Next, either trimmed, LCO-treated wild-type *Populus* roots (Figures 8 and 9), or untrimmed and untreated wild-type or RNAi *Populus* roots (Figure 10) were placed on top of the hyphae-covered cellophane and sandwiched in place with an additional sheet of cellophane placed on top. *Populus* plants cocultured with *L. bicolor* were grown for 3 weeks in the growth chamber and then destructively harvested. Undisturbed ECM roots were identified using a stereomicroscope (Leica M165 FC) and subsequently imaged. The number of individual lateral roots with a distinct fungal mantle (as shown in Figures 8A and 10A) or without per length of primary root was determined. A subset of ECM roots tips was removed from the rest of the roots system with a scalpel for further analysis using confocal microscopy

Microscopic Analysis of ECM Roots

ECM lateral roots were fixed in 4% paraformaldehyde overnight at 4°C, washed three times in PBS, and then embedded in 6% agarose as described previously by Felten et al. (2009). Using a vibratome (1000 Plus), ten 50-μm cross sections were taken beginning ~500 μm behind the root tip to ensure sampling of uniformly colonized root tissue. The cross sections were then immersed in PBS with 2 μg mL^{-1} wheat germ agglutinin conjugated to Alexa Fluor 488 (Invitrogen) and 10 μg mL^{-1} propidium iodide (MP Biomedicals). After overnight incubation at 4°C, stained cross sections were rinsed with PBS and mounted on microscope slides in PBS for immediate observation with an LSM780 confocal laser scanning microscope (Carl Zeiss) equipped with an LD C-Apochromat 40×/1.1-W Korr M27 objective. Wheat germ agglutinin-Alexa Fluor 488 and propidium iodide were excited with the 488-nm line of an argon laser. Emission was detected between 493 and 534 nm for wheat germ agglutinin-Alexa Fluor 488 and between 622 and 702 nm for propidium iodide. The images were acquired with a scanning resolution of 1024 × 1024 pixels. Settings (laser intensity, gain, offset, magnification, airy units) were similar for all sample observations. Images of ECM cross sections were analyzed using ImageJ (http://imagej.nih.gov/) to determine average root diameter from two perpendicular measurements, average mantle width from four separate measurements equidistant from one another along the mantle, root circumference as measured from the outer tip of root epidermal cells, and the Hartig net boundary as shown in Figures 9 and 10.

Inoculation of *Populus* with AM Fungi and Measurement of Colonization

For the colonization assays with AM fungi only, the sterile wild-type and RNAi *Populus* (*Populus tremula* × *Populus alba* clone INRA 717-1B4) lines were grown in axenic conditions in half-strength MS medium, pH 5.5, in magenta boxes (Sigma-Aldrich) under a 16-h photoperiod at 25 ± 1°C for 4 to 6 weeks prior to inoculation with AM fungi. The same *Populus* lines were also acclimated to greenhouse conditions in a peat:vermiculite soil substrate (7:3, v/v) in a 165-mL leach tube under a 16-h photoperiod at 25 ± 1°C for 4 weeks before inoculation. *Rhizophagus irregularis* DAOM 197198 (syn: *Glomus intraradices*; Stockinger et al., 2009; Tisserant et al., 2012) was maintained in axenic carrot root organ cultures. Germinated spores were produced as described by Chabot et al. (1992). Two independent experiments of inoculation with *Rhizophagus irregularis* were performed, one in axenic in vitro conditions and the other in the greenhouse. A set of plants grown separately under identical conditions, but without *Rhizophagus irregularis* inoculation, served as controls (four plants per line). For

the axenic in vitro experiment, four 6-week-old plants were inoculated with *Rhizophagus irregularis* (100 spores per plant) in magenta boxes with 100 mL of half-strength MS medium, pH 5.5, under a 16-h photoperiod at 25 ± 1°C for 6 weeks. For the greenhouse experiment, four 4-week-old plants were inoculated with *Rhizophagus irregularis* (800 spores per plant) in 1-liter pots with a twice-autoclaved peat;vermiculite mixture (7:3, v/v) under a 16-h photoperiod at 25 ± 1°C for 4 weeks. Greenhouse plants were irrigated twice weekly with half-strength BandD solution, pH 5.5 (Broughton and Dilworth, 1971), containing a low concentration of potassium phosphate (10 μM, K_2HPO_4) to favor AM colonization (Smith et al., 2003). Six weeks following inoculation, plants were harvested and the root systems were rinsed with deionized sterile water. Roots were sampled for staining with trypan blue according to a modified staining procedure by Koske and Gemma (1989). The stained roots were observed under a light microscope (Carl Zeiss) to determine the percentage of both arbuscular and root length colonization following the gridline-intersect method (McGonigle et al., 1990).

Determination of Root Growth and Ectomycorrhiza Formation in *Pinus pinaster* Treated with LCOs

Seeds of maritime pine (*Pinus pinaster*, Landes-Sore-VG source) were surface sterilized with 37% H_2O_2 for 30 min and sown on Petri dishes containing 1% agarose. Two weeks later, germinated seeds were transferred individually into square Petri dishes containing solid modified MMN medium (3.67 mM KH_2PO_4, 0.45 M $CaCl_2$, 0.43 M NaCl, 0.22 M $(NH_4)_2HPO_4$, and 0.61 mM $MgSO_4 \cdot 7\,H_2O$; micronutrient solution, 2.5 g L^{-1} Glc, pH 5.5, and 10 g L^{-1} agarose) between two layers of damp germination paper (Supplemental Figure 16). Two days later, seedlings were treated either with 1 mL of 10^{-8} M nsLCOs or sLCOs or with 1 mL of mock treatment (0.005% ethanol). After 3 weeks of growth, the number of lateral roots per plant and the length of the primary root were determined from images of the root system using ImageJ software (https://imagej.nih.gov/ij/). Ectomycorrhizas were produced using a similar setup (Supplemental Figure 17). After plants were placed in square Petri dishes, six plugs of the ECM fungus *Hebeloma cylindrosporum* (homokaryotic strain h7; Debaud and Gay, 1987) grown on solid yeast extract, malt extract, and glucose medium (Garcia et al., 2014) were placed beside the primary root. These cocultures were treated either with 1 mL of 10^{-8} M nsLOCs or sLCOs or with 1 mL of mock treatment (0.005% ethanol). Three weeks later, the number of ectomycorrhizas per plant was recorded.

Statistical Analyses

Raw data from the Ca^{2+} spiking experiments were used directly for statistical analysis. By contrast, for the lateral root and colonization experiments, the data were normalized to the wild-type control to account for variation between experiments replicated in time. All data were analyzed using R (version 3.2.4; http://www.R-project.org/). Welch's two-sample *t* test was used for comparing two treatments, while one-way ANOVA (see Supplemental File) and Tukey pairwise comparisons ($P \leq 0.05$) were used for comparing three or more treatments.

Supplemental Data

Supplemental Figure 1. Quantification of root hair branching frequency in *medicago truncatula* and *vicia sativa* roots.

Supplemental Figure 2. HPLC chromatogram showing the synthetic standard LCO-IV, C18:1.

Supplemental Figure 3. HPLC chromatogram showing the LCO-IV, C18:1, from *laccaria bicolor* sample (A7).

Supplemental Figure 4. HPLC chromatogram showing the LCO-V, C18:1 from *laccaria bicolor* sample (A7).

Supplemental Figure 5. HPLC chromatogram showing the LCO-IV, C18:1, NMe from *laccaria bicolor* sample (A7).

Supplemental Figure 6. HPLC chromatograms showing LCO-IV, C18:1 and LCO-III, C18:1, NMe Cb Fuc from *Laccaria bicolor* sample (A7).

Supplemental Figure 7. U-HPLC chromatograms showing the synthetic standards of sulfated and nonsulfated LCO-IV, C18:1.

Supplemental Figure 8. U-HPLC chromatogram showing the sulfated and the nonsulfated LCO-IV, C18:1 N-Me from *laccaria bicolor* sample (MP-B1C).

Supplemental Figure 9. Root hair branching assay in *populus* roots.

Supplemental Figure 10. Images of wild-type *populus* transformed with DsRed and green-GECO.

Supplemental Figure 11. Normalized gene expression in *populus* RNA interference lines.

Supplemental Figure 12. Normalized gene expression of *CASTOR* and *POLLUX* in candidate *CASTOR*- and *POLLUX*-RNA interference lines.

Supplemental Figure 13. Normalized gene expression of *CASTOR*, *POLLUX*, and *CCaMK* in RNAi lines of *populus* compared with wild-type.

Supplemental Figure 14. Images of three independent events of CASTOR/POLLUX-RNAi *populus* transformed with DsRed and green-GECO.

Supplemental Figure 15. Arbuscular mycorrhizal–*populus* colonization assays with wild-type, *CASTOR*/*POLLUX*-RNAi and *CCaMK*-RNAi lines.

Supplemental Figure 16. Effect of LCOs on lateral root development in *pinus pinaster*.

Supplemental Figure 17. Effect of LCOs on ectomycorrhiza formation in *pinus pinaster*.

Supplemental Table 1. Summary of lipochitooligosaccharides detected in the medium of 17 independent cultures of *laccaria bicolor*.

Supplemental Table 2. RNA interference constructs used for knocking down the expression of *CASTORa*/*b*, *POLLUXa*/*b*, and *CCaMKa*/*b.*

Supplemental Table 3. Primers used for PCR and RT-qPCR in this study.

Supplemental Movie 1. Calcium spiking in atrichoblasts from wild-type *populus* roots expressing nucleus-localized G-GECO observed 20 min following application of germinating spore exudates from the arbuscular mycorrhizal fungus *rhizophagus irregularis*.

Supplemental Movie 2. Absence of calcium spiking in atrichoblasts from wild-type *populus* roots expressing nucleus-localized G-GECO observed 20 min following application of mock treatment with water containing 0.005% ethanol.

Supplemental Movie 3. Calcium spiking in atrichoblasts from wild-type *populus* roots expressing nucleus-localized G-GECO observed 20 min following application of nonsulfated lipochitooligosaccharides (10^{-7} M).

Supplemental Movie 4. Calcium spiking in atrichoblasts from wild-type *populus* roots expressing nucleus-localized G-GECO observed 20 min following application of sulfated lipochitooligosaccharides (10^{-7} M).

Supplemental Movie 5. Calcium spiking in atrichoblasts from wild-type *populus* roots expressing nucleus-localized G-GECO observed 20 min following application of tetra-*N*-acetyl chitotetraose (10^{-6} M).

Supplemental Movie 6. Calcium spiking in atrichoblasts from wild-type *populus* roots expressing nucleus-localized G-GECO observed 20 min following application of germinating spore exudates from the arbuscular mycorrhizal fungus *rhizophagus irregularis*.

Supplemental Movie 7. Reduced calcium spiking in atrichoblasts of CASTOR/POLLUX-RNAi *populus* roots expressing nucleus-localized G-GECO observed 20 min following application of germinating spore exudates from the arbuscular mycorrhizal fungus *rhizophagus irregularis*.

Supplemental Movie 8. Minor induction of calcium spiking in atrichoblasts from wild-type *populus* roots expressing nucleus-localized G-GECO observed 20 min following application of hyphal exudates from *laccaria bicolor*.

Supplemental Movie 9. Calcium spiking in atrichoblasts from wild-type *populus* roots expressing nucleus-localized G-GECO observed 20 min following application of hyphae from the ectomycorrhizal fungus *laccaria bicolor*.

Supplemental Movie 10. Spiking in atrichoblasts from wild-type *populus* roots expressing nucleus-localized G-GECO observed 20 min following application of germinating spore exudates from the arbuscular mycorrhizal fungus *rhizophagus irregularis*.

Supplemental Movie 11. Absence of calcium spiking in atrichoblasts from wild-type *populus* roots expressing the nucleus-localized G-GECO observed 20 min following application of mock treatment with water containing 0.005% ethanol.

Supplemental Movie 12. Calcium spiking in atrichoblasts from wild-type *populus* roots expressing nucleus-localized G-GECO observed 20 min following application of hyphae from the ectomycorrhizal fungus *laccaria bicolor*.

Supplemental Movie 13. Absence of calcium spiking in atrichoblasts from CASTOR/POLLUX-RNAi *populus* roots expressing the nucleus-localized G-GECO observed 20 min following application of hyphae from the ectomycorrhizal fungus *laccaria bicolor*.

Supplemental Movie 14. Induction of calcium spiking in trichoblasts from wild-type *populus* roots expressing nucleus-localized G-GECO observed immediately following application of nsLCOs (10^{-9} M).

Supplemental File. ANOVA tables.

ACKNOWLEDGMENTS

We thank Sarah Swanson for training and support with confocal microscopy techniques, Francis Martin for providing *L. bicolor* strain S238N, Giles Oldroyd for providing the binary vector pEC11579 carrying G-GECO, Fabienne Maillet for providing purified sLCOs and nsLCOs, and Hugues Driguez for providing synthetic LCO standards for mass spectrometry. Financial support for this project was primarily provided by the USDA (grant WIS01695) and National Science Foundation (NSF; grant DGE-1256259). Additional financial support was provided by the U.S. Department of Energy (DOE; grant DE-SC0018247) and NSF (grants 1546742 and 1331098) for partial analysis of Ca^{2+} spiking; the French Agence Nationale de la Recherche (contract ANR-14-CE18-0008-01) and the Laboratoire d'Excellence entitled TULIP (grant ANR-10-LABX-41) for the mass spectrometry analyses with additional support from the ICT-Mass Spectrometry and MetaToul facilities, and from the MetaboHUB-ANR-11-INBS-0010 network; the Tree Genomics and Biosafety Cooperative at Oregon State University and the NSF Center for Advanced Forestry Systems (grant 1238305) for partial support of RNAi line development; the Plant–Microbe Interfaces Scientific Focus Area in the Genomic Science Program, the Office of Biological and Environmental Research in the DOE Office of Science (Oak Ridge National Laboratory is managed by UT-Battelle, LLC, the DOE (contract DE-AC05-00OR22725) for the AM colonization assays; and from the USDA (grant 2017-67014-26530 to H.B.).

AUTHOR CONTRIBUTIONS

K.R.C., M.V., S.H.S., G.B., V.P.-P., and J.-M.A. designed the research; K.R.C., A.B., T.B.I., M.V., J.M., K.G., T.A.R., C.M., J.L., S.J., J.S., K.G.S., N.S. P.J., and F.M. performed the experiments; K.R.C., A.B., M.V., J.M., E.S., E.F., Y.W., P.J., G.B., V.P.-P., and J.-M.A. analyzed the data; and K.R.C. wrote the article with input from A.B., M.V., K.G., J.L., H.B., S.H.S., G.B., P.J., V.P.-P., and J.-M.A.

Received September 10, 2018; revised May 17, 2019; accepted August 6, 2019; published October 15, 2019.

REFERENCES

Akiyama, K., and Hayashi, H. (2006). Strigolactones: Chemical signals for fungal symbionts and parasitic weeds in plant roots. Ann. Bot. **97:** 925–931.

Akiyama, K., Matsuzaki, K., and Hayashi, H. (2005). Plant sesquiterpenes induce hyphal branching in arbuscular mycorrhizal fungi. Nature **435:** 824–827.

Ané, J.-M., et al. (2004). *Medicago truncatula DMI1* required for bacterial and fungal symbioses in legumes. Science **303:** 1364–1367.

Ardourel, M., Lortet, G., Maillet, F., Roche, P., Truchet, G., Promé, J.-C., and Rosenberg, C. (1995). In *Rhizobium meliloti*, the operon associated with the nod box n5 comprises nodL, noeA and noeB, three host-range genes specifically required for the nodulation of particular *Medicago* species. Mol. Microbiol. **17:** 687–699.

Balestrini, R., and Bonfante, P. (2014). Cell wall remodeling in mycorrhizal symbiosis: A way towards biotrophism. Front. Plant Sci. **5:** 237.

Berbee, M.L., and Taylor, J.W. (1993). Dating the evolutionary radiations of the true fungi. Can. J. Bot. **71:** 1114–1127.

Besserer, A., Puech-Pagès, V., Kiefer, P., Gomez-Roldan, V., Jauneau, A., Roy, S., Portais, J.C., Roux, C., Bécard, G., and Séjalon-Delmas, N. (2006). Strigolactones stimulate arbuscular mycorrhizal fungi by activating mitochondria. PLoS Biol. **4:** e226.

Besserer, A., Bécard, G., Jauneau, A., Roux, C., and Séjalon-Delmas, N. (2008). GR24, a synthetic analog of strigolactones, stimulates the mitosis and growth of the arbuscular mycorrhizal fungus *Gigaspora rosea* by boosting its energy metabolism. Plant Physiol. **148:** 402–413.

Bhuvaneswari, T.V., and Solheim, B. (1985). Root hair deformation in the white clover/*Rhizobium trifolii* symbiosis. Physiol. Plant **63:** 25–34.

Bonfante, P., and Genre, A. (2010). Mechanisms underlying beneficial plant-fungus interactions in mycorrhizal symbiosis. Nat. Commun. **1:** 48.

Bravo, A., York, T., Pumplin, N., Mueller, L.A., and Harrison, M.J. (2016). Genes conserved for arbuscular mycorrhizal symbiosis identified through phylogenomics. Nat. Plants **2:** 15208.

Broughton, W.J., and Dilworth, M.J. (1971). Control of leghaemoglobin synthesis in snake beans. Biochem. J. **125:** 1075–1080.

Brundrett, M.C. (2002). Coevolution of roots and mycorrhizas of land plants. New Phytol. **154:** 275–304.

Brundrett, M.C., and Tedersoo, L. (2018). Evolutionary history of mycorrhizal symbioses and global host plant diversity. New Phytol. **220:** 1108–1115.

Capoen, W., Sun, J., Wysham, D., Otegui, M.S., Venkateshwaran, M., Hirsch, S., Miwa, H., Downie, J.A., Morris, R.J., Ané, J.-M., and Oldroyd, G.E.D. (2011). Nuclear membranes control symbiotic calcium signaling of legumes. Proc. Natl. Acad. Sci. USA **108:** 14348–14353.

Casieri, L., et al. (2013). Biotrophic transportome in mutualistic plant-fungal interactions. Mycorrhiza **23:** 597–625.

Chabaud, M., Genre, A., Sieberer, B.J., Faccio, A., Fournier, J., Novero, M., Barker, D.G., and Bonfante, P. (2011). Arbuscular mycorrhizal hyphopodia and germinated spore exudates trigger Ca^{2+} spiking in the legume and nonlegume root epidermis. New Phytol. **189:** 347–355.

Chabot, S., Becard, G., and Piche, Y. (1992). Life cycle of *Glomus intraradix* in root organ culture. Mycologia **84:** 315–321.

Charpentier, M., Bredemeier, R., Wanner, G., Takeda, N., Schleiff, E., and Parniske, M. (2008). *Lotus japonicus* CASTOR and POLLUX are ion channels essential for perinuclear calcium spiking in legume root endosymbiosis. Plant Cell **20:** 3467–3479.

Charpentier, M., Sun, J., Vaz Martins, T., Radhakrishnan, G.V., Findlay, K., Soumpourou, E., Thouin, J., Véry, A.-A., Sanders, D., Morris, R.J., and Oldroyd, G.E.D. (2016). Nuclear-localized cyclic nucleotide-gated channels mediate symbiotic calcium oscillations. Science **352:** 1102–1105.

Chen, C., Fan, C., Gao, M., and Zhu, H. (2009). Antiquity and function of CASTOR and POLLUX, the twin ion channel-encoding genes key to the evolution of root symbioses in plants. Plant Physiol. **149:** 306–317.

Choi, J., Summers, W., and Paszkowski, U. (2018). Mechanisms underlying establishment of arbuscular mycorrhizal symbioses. Annu. Rev. Phytopathol. **56:** 135–160.

Cissoko, M., et al. (2018). Actinorhizal signaling molecules: *Frankia* root hair deforming factor shares properties with NIN inducing factor. Front. Plant Sci. **9:** 1494.

Dauphin, A., Gérard, J., Lapeyrie, F., and Legué, V. (2007). Fungal hypaphorine reduces growth and induces cytosolic calcium increase in root hairs of *Eucalyptus globulus*. Protoplasma **231:** 83–88.

Debaud, J.C., and Gay, G. (1987). In vitro fruiting under controlled conditions of the ectomycorrhizal fungus *Hebeloma cylindrosporum* associated with *Pinus pinaster.* New Phytol. **105:** 429–435.

Delaux, P.M., Séjalon-Delmas, N., Bécard, G., and Ané, J.M. (2013). Evolution of the plant-microbe symbiotic 'toolkit'. Trends Plant Sci. **18:** 298–304.

Delaux, P.M., Varala, K., Edger, P.P., Coruzzi, G.M., Pires, J.C., and Ané, J.M. (2014). Comparative phylogenomics uncovers the impact of symbiotic associations on host genome evolution. PLoS Genet. **10:** e1004487.

Ditengou, F.A., Béguiristain, T., and Lapeyrie, F. (2000). Root hair elongation is inhibited by hypaphorine, the indole alkaloid from the ectomycorrhizal fungus *Pisolithus tinctorius*, and restored by indole-3-acetic acid. Planta **211:** 722–728.

Ehrhardt, D.W., Wais, R., and Long, S.R. (1996). Calcium spiking in plant root hairs responding to *Rhizobium* nodulation signals. Cell **85:** 673–681.

El Yahyaoui, F., Küster, H., Ben Amor, B., Hohnjec, N., Pühler, A., Becker, A., Gouzy, J., Vernié, T., Gough, C., Niebel, A., Godiard, L., and Gamas, P. (2004). Expression profiling in Medicago truncatula identifies more than 750 genes differentially expressed during nodulation, including many potential regulators of the symbiotic program. Plant Physiol. **136:** 3159–3176.

Fåhraeus, G. (1957). The infection of clover root hairs by nodule bacteria studied by a simple glass slide technique. J. Gen. Microbiol. **16:** 374–381.

Feijen, F.A.A., Vos, R.A., Nuytinck, J., and Merckx, V.S.F.T. (2018). Evolutionary dynamics of mycorrhizal symbiosis in land plant diversification. Sci. Rep. **8:** 10698.

Felten, J., Kohler, A., Morin, E., Bhalerao, R.P., Palme, K., Martin, F., Ditengou, F.A., and Legué, V. (2009). The ectomycorrhizal fungus *Laccaria bicolor* stimulates lateral root formation in poplar and Arabidopsis through auxin transport and signaling. Plant Physiol. **151:** 1991–2005.

Felten, J., Legué, V., and Ditengou, F.A. (2010). Lateral root stimulation in the early interaction between *Arabidopsis thaliana* and the ectomycorrhizal fungus *Laccaria bicolor*: Is fungal auxin the trigger? Plant Signal. Behav. **5:** 864–867.

Filichkin, S.A., Meilan, R., Busov, V.B., Ma, C., Brunner, A.M., and Strauss, S.H. (2006). Alcohol-inducible gene expression in transgenic *Populus.* Plant Cell Rep. **25:** 660–667.

Fusconi, A. (2014). Regulation of root morphogenesis in arbuscular mycorrhizae: What role do fungal exudates, phosphate, sugars and hormones play in lateral root formation? Ann. Bot. **113:** 19–33.

Garcia, K., and Zimmermann, S.D. (2014). The role of mycorrhizal associations in plant potassium nutrition. Front. Plant Sci. **5:** 337.

Garcia, K., Delteil, A., Conéjéro, G., Becquer, A., Plassard, C., Sentenac, H., and Zimmermann, S. (2014). Potassium nutrition of ectomycorrhizal *Pinus pinaster*: Overexpression of the *Hebeloma cylindrosporum* HcTrk1 transporter affects the translocation of both $K(^{+})$ and phosphorus in the host plant. New Phytol. **201:** 951–960.

Garcia, K., Delaux, P.M., Cope, K.R., and Ané, J.M. (2015). Molecular signals required for the establishment and maintenance of ectomycorrhizal symbioses. New Phytol. **208:** 79–87.

Garcia, K., Chasman, D., Roy, S., and Ané, J.-M. (2017). Physiological responses and gene co-expression network of mycorrhizal roots under K^{+} deprivation. Plant Physiol. **173:** 1811–1823.

Gay, G., Normand, L., Marmeisse, R., Sotta, B., and Debaud, J.C. (1994). Auxin overproducer mutants of *Hebeloma cylindrosporum* Romagnesi have increased mycorrhizal activity. New Phytol. **128:** 645–657.

Genre, A., Chabaud, M., Balzergue, C., Puech-Pagès, V., Novero, M., Rey, T., Fournier, J., Rochange, S., Bécard, G., Bonfante, P., and Barker, D.G. (2013). Short-chain chitin oligomers from arbuscular mycorrhizal fungi trigger nuclear Ca^{2+} spiking in *Medicago truncatula* roots and their production is enhanced by strigolactone. New Phytol. **198:** 190–202.

Gomez-Roldan, V., et al. (2008). Strigolactone inhibition of shoot branching. Nature **455:** 189–194.

Groten, K., Pahari, N.T., Xu, S., Miloradovic van Doorn, M., and Baldwin, I.T. (2015). Virus-induced gene silencing using Tobacco Rattle Virus as a tool to study the interaction between *Nicotiana attenuata* and *Rhizophagus irregularis.* PLoS One **10:** e0136234.

Gutjahr, C., and Paszkowski, U. (2013). Multiple control levels of root system remodeling in arbuscular mycorrhizal symbiosis. Front. Plant Sci. **4:** 204.

Gutjahr, C., Casieri, L., and Paszkowski, U. (2009). *Glomus intraradices* induces changes in root system architecture of rice independently of common symbiosis signaling. New Phytol. **182:** 829–837.

Han, K.H., Meilan, R., Ma, C., and Strauss, S.H. (2000). An Agrobacterium tumefaciens transformation protocol effective on a variety of cottonwood hybrids (genus Populus). Plant Cell Rep. **19:** 315–320.

Heckman, D.S., Geiser, D.M., Eidell, B.R., Stauffer, R.L., Kardos, N.L., and Hedges, S.B. (2001). Molecular evidence for the early colonization of land by fungi and plants. Science **293:** 1129–1133.

Heidstra, R., Geurts, R., Franssen, H., Spaink, H.P., Van Kammen, A., and Bisseling, T. (1994). Root hair deformation activity of nodulation factors and their fate on *Vicia sativa.* Plant Physiol. **105:** 787–797.

Hibbett, D.S., and Matheny, P.B. (2009). The relative ages of ectomycorrhizal mushrooms and their plant hosts estimated using Bayesian relaxed molecular clock analyses. BMC Biol. **7:** 13.

Hoeksema, J.D., et al. (2018). Evolutionary history of plant hosts and fungal symbionts predicts the strength of mycorrhizal mutualism. Commun. Biol. **1:** 116.

Horváth, B., et al. (2011). *Medicago truncatula IPD3* is a member of the common symbiotic signaling pathway required for rhizobial and mycorrhizal symbioses. Mol. Plant Microbe Interact. **24:** 1345–1358.

Ivanchenko, M.G., Muday, G.K., and Dubrovsky, J.G. (2008). Ethylene-auxin interactions regulate lateral root initiation and emergence in *Arabidopsis thaliana.* Plant J. **55:** 335–347.

Jargeat, P., Chaumeton, J.P., Navaud, O., Vizzini, A., and Gryta, H. (2014). The *Paxillus involutus* (Boletales, Paxillaceae) complex in Europe: Genetic diversity and morphological description of the new species *Paxillus cuprinus*, typification of *P. involutus* s.s., and synthesis of species boundaries. Fungal Biol. **118:** 12–31.

Jeffries, P., Gianinazzi, S., Perotto, S., Turnau, K., and Barea, J.M. (2003). The contribution of arbuscular mycorrhizal fungi in sustainable maintenance of plant health and soil fertility. Biol. Fertil. Soils **37:** 1–16.

Kafle, A., Cope, K., Raths, R., Krishna Yakha, J., Subramanian, S., Bücking, H., and Garcia, K. (2019). Harnessing soil microbes to improve plant phosphate efficiency in cropping systems. Agronomy **9:** 127.

Kamel, L., Keller-Pearson, M., Roux, C., and Ané, J.M. (2017). Biology and evolution of arbuscular mycorrhizal symbiosis in the light of genomics. New Phytol. **213:** 531–536.

Karabaghli-Degron, C., Sotta, B., Bonnet, M., and Gay, G. (1998). The auxin transport inhibitor 2,3,5-triiodobenzoic acid (TIBA) inhibits the stimulation of in vitro lateral root formation and the colonization of the tap-root cortex of Norway spruce (*Picea abies*) seedlings by the ectomycorrhizal fungus. New Phytol. **140:** 723–733.

Kelner, A., Leitão, N., Chabaud, M., Charpentier, M., and de Carvalho-Niebel, F. (2018). Dual color sensors for simultaneous analysis of calcium signal dynamics in the nuclear and cytoplasmic compartments of plant cells. Front. Plant Sci. **9:** 245.

Kevei, Z., et al. (2007). 3-Hydroxy-3-methylglutaryl coenzyme a reductase 1 interacts with NORK and is crucial for nodulation in *Medicago truncatula.* Plant Cell **19:** 3974–3989.

Kohler, A., et al.; Mycorrhizal Genomics Initiative Consortium (2015). Convergent losses of decay mechanisms and rapid turnover of symbiosis genes in mycorrhizal mutualists. Nat. Genet. **47:** 410–415.

Koske, R.E., and Gemma, J.N. (1989). A modified procedure for staining roots to detect VA mycorrhizas. Mycol. Res. **92:** 486–488.

Krebs, M., Held, K., Binder, A., Hashimoto, K., Den Herder, G., Parniske, M., Kudla, J., and Schumacher, K. (2012). FRET-based genetically encoded sensors allow high-resolution live cell imaging of Ca^{2+} dynamics. Plant J. **69:** 181–192.

Kretzschmar, T., Kohlen, W., Sasse, J., Borghi, L., Schlegel, M., Bachelier, J.B., Reinhardt, D., Bours, R., Bouwmeester, H.J., and Martinoia, E. (2012). A petunia ABC protein controls strigolactone-dependent symbiotic signalling and branching. Nature **483:** 341–344.

Lagrange, H., Jay-Allgmand, C., and Lapeyrie, F. (2001). Rutin, the phenolglycoside from eucalyptus root exudates, stimulates *Pisolithus* hyphal growth at picomolar concentrations. New Phytol. **149:** 349–355.

Lazo, G.R., Stein, P.A., and Ludwig, R.A. (1991). A DNA transformation-competent *Arabidopsis* genomic library in *Agrobacterium.* Biotechnology (N Y) **9:** 963–967.

Lepage, B., Currah, R., Stockey, R., and Rothwell, G. (1997). Fossil ectomycorrhizae from the middle Eocene. Am. J. Bot. **84:** 410–412.

Lerouge, P., Roche, P., Faucher, C., Maillet, F., Truchet, G., Promé, J.C., and Dénarié, J. (1990). Symbiotic host-specificity of *Rhizobium meliloti* is determined by a sulphated and acylated glucosamine oligosaccharide signal. Nature **344:** 781–784.

Lévy, J., et al. (2004). A putative Ca^{2+} and calmodulin-dependent protein kinase required for bacterial and fungal symbioses. Science **303:** 1361–1364.

Luginbuehl, L.H., and Oldroyd, G.E.D. (2017). Understanding the arbuscule at the heart of endomycorrhizal symbioses in plants. Curr. Biol. **27:** R952–R963.

MacLean, A.M., Bravo, A., and Harrison, M.J. (2017). Plant signaling and metabolic pathways enabling arbuscular mycorrhizal symbiosis. Plant Cell **29:** 2319–2335.

Maillet, F., et al. (2011). Fungal lipochitooligosaccharide symbiotic signals in arbuscular mycorrhiza. Nature **469:** 58–63.

Martin, F., et al. (2008). The genome of *Laccaria bicolor* provides insights into mycorrhizal symbiosis. Nature **452:** 88–92.

Martin, F., Kohler, A., Murat, C., Veneault-Fourrey, C., and Hibbett, D.S. (2016). Unearthing the roots of ectomycorrhizal symbioses. Nat. Rev. Microbiol. **14:** 760–773.

Martin, F.M., Uroz, S., and Barker, D.G. (2017). Ancestral alliances: Plant mutualistic symbioses with fungi and bacteria. Science **356:** eaad4501.

McGonigle, T.P., Miller, M.H., Evans, D.G., Fairchild, G.L., and Swan, J.A. (1990). A new method which gives an objective measure of colonization of roots by vesicular—arbuscular mycorrhizal fungi. New Phytol. **115:** 495–501.

Messinese, E., Mun, J.-H., Yeun, L.H., Jayaraman, D., Rougé, P., Barre, A., Lougnon, G., Schornack, S., Bono, J.-J., Cook, D.R., and Ané, J.-M. (2007). A novel nuclear protein interacts with the symbiotic DMI3 calcium- and calmodulin-dependent protein kinase of *Medicago truncatula.* Mol. Plant Microbe Interact. **20:** 912–921.

Miyata, K., et al. (2014). The bifunctional plant receptor, OsCERK1, regulates both chitin-triggered immunity and arbuscular mycorrhizal symbiosis in rice. Plant Cell Physiol. **55:** 1864–1872.

Morandi, D., Prado, E., Sagan, M., and Duc, G. (2005). Characterisation of new symbiotic *Medicago truncatula* (Gaertn.) mutants, and phenotypic or genotypic complementary information on previously described mutants. Mycorrhiza **15:** 283–289.

Mukherjee, A., and Ané, J.-M. (2011). Germinating spore exudates from arbuscular mycorrhizal fungi: Molecular and developmental responses in plants and their regulation by ethylene. Mol. Plant Microbe Interact. **24:** 260–270.

Müller, A., Volmer, K., Mishra-Knyrim, M., and Polle, A. (2013). Growing poplars for research with and without mycorrhizas. Front. Plant Sci. **4:** 332.

Negi, S., Sukumar, P., Liu, X., Cohen, J.D., and Muday, G.K. (2010). Genetic dissection of the role of ethylene in regulating auxin-dependent lateral and adventitious root formation in tomato. Plant J. **61:** 3–15.

Nehls, U. (2008). Mastering ectomycorrhizal symbiosis: The impact of carbohydrates. J. Exp. Bot. **59:** 1097–1108.

Oláh, B., Brière, C., Bécard, G., Dénarié, J., and Gough, C. (2005). Nod factors and a diffusible factor from arbuscular mycorrhizal fungi

stimulate lateral root formation in *Medicago truncatula* via the DMI1/DMI2 signalling pathway. Plant J. **44:** 195–207.

Op den Camp, R., Streng, A., De Mita, S., Cao, Q., Polone, E., Liu, W., Ammiraju, J.S.S., Kudrna, D., Wing, R., Untergasser, A., Bisseling, T., and Geurts, R. (2011). LysM-type mycorrhizal receptor recruited for rhizobium symbiosis in nonlegume *Parasponia*. Science **331:** 909–912.

Pan, Y., Birdsey, R.A., Phillips, O.L., and Jackson, R.B. (2013). The structure, distribution, and biomass of the world's forests. Annu. Rev. Ecol. Evol. Syst. **44:** 593–622.

Peiter, E., et al. (2007). The *Medicago truncatula* DMI1 protein modulates cytosolic calcium signaling. Plant Physiol. **145:** 192–203.

Pellegrin, C., Daguerre, Y., Ruytinx, J., Guinet, F., Kemppainen, M., Plourde, M.B., Hecker, A., Morin, E., Pardo, A.G., Germain, H., Martin, F.M., and Veneault-Fourrey, C. (2017). *Laccaria bicolor* MiSSP8 is a small-secreted protein decisive for the establishment of the ectomycorrhizal symbiosis. bioRxiv ●●●: 218131.

Plett, J.M., et al. (2017). *Populus trichocarpa* encodes small, effector-like secreted proteins that are highly induced during mutualistic symbiosis. Sci. Rep. **7:** 382.

Plett, J.M., and Martin, F. (2012). Poplar root exudates contain compounds that induce the expression of MiSSP7 in *Laccaria bicolor*. Plant Signal. Behav. **7:** 12–15.

Plett, J.M., Kemppainen, M., Kale, S.D., Kohler, A., Legué, V., Brun, A., Tyler, B.M., Pardo, A.G., and Martin, F. (2011). A secreted effector protein of *Laccaria bicolor* is required for symbiosis development. Curr. Biol. **21:** 1197–1203.

Plett, J.M., Tisserant, E., Brun, A., Morin, E., Grigoriev, I.V., Kuo, A., Martin, F., and Kohler, A. (2015). The mutualist *Laccaria bicolor* expresses a core gene regulon during the colonization of diverse host plants and a variable regulon to counteract host-specific defenses. Mol. Plant Microbe Interact. **28:** 261–273.

Poinsot, V., Crook, M.B., Erdn, S., Maillet, F., Bascaules, A., and Ané, J.M. (2016). New insights into Nod factor biosynthesis: Analyses of chitooligomers and lipo-chitooligomers of *Rhizobium* sp. IRBG74 mutants. Carbohydr. Res. **434:** 83–93.

Price, N.P.J., Relić, B., Talmont, F., Lewin, A., Promé, D., Pueppke, S.G., Maillet, F., Dénarié, J., Promé, J.C., and Broughton, W.J. (1992). Broad-host-range *Rhizobium* species strain NGR234 secretes a family of carbamoylated, and fucosylated, nodulation signals that are O-acetylated or sulphated. Mol. Microbiol. **6:** 3575–3584.

Redecker, D., Kodner, R., and Graham, L.E. (2000). Glomalean fungi from the Ordovician. Science **289:** 1920–1921.

Remy, W., Taylor, T.N., Hass, H., and Kerp, H. (1994). Four hundred-million-year-old vesicular arbuscular mycorrhizae. Proc. Natl. Acad. Sci. USA **91:** 11841–11843.

Rupp, L.A., and Mudge, K.W. (1985). Ethephon and auxin induce mycorrhiza-like changes in the morphology of root organ cultures of mugo pine. Physiol. Plant. **64:** 316–322.

Rupp, L.a., Mudge, K.W., and Negm, F.B. (1989). Involvement of ethylene in ectomycorrhiza formation and dichotomous branching of roots of mugo pine seedlings. Can. J. Bot. **67:** 477–482.

Singh, S., and Parniske, M. (2012). Activation of calcium- and calmodulin-dependent protein kinase (CCaMK), the central regulator of plant root endosymbiosis. Curr. Opin. Plant Biol. **15:** 444–453.

Smith, S.E., and Read, D. (2010). Mycorrhizal Symbiosis. (London: Academic Press).

Smith, S.E., Smith, F.A., and Jakobsen, I. (2003). Mycorrhizal fungi can dominate phosphate supply to plants irrespective of growth responses. Plant Physiol. **133:** 16–20.

Son, S.H., and Hall, R.B. (1990). Multiple shoot regeneration from root organ cultures of *Populus alba* x *P. grandidentata.* Plant Cell Tissue Organ Cult. **20:** 53–57.

Spatafora, J.W., et al. (2016). A phylum-level phylogenetic classification of zygomycete fungi based on genome-scale data. Mycologia **108:** 1028–1046.

Spatafora, J.W., Aime, M.C., Grigoriev, I.V., Martin, F., Stajich, J.E., and Blackwell, M. (2017). The fungal tree of life: From molecular systematics to genome-scale phylogenies. Microbiol. Spectr. **5:** 3–34.

Splivallo, R., Fischer, U., Göbel, C., Feussner, I., and Karlovsky, P. (2009). Truffles regulate plant root morphogenesis via the production of auxin and ethylene. Plant Physiol. **150:** 2018–2029.

Steinkellner, S., Lendzemo, V., Langer, I., Schweiger, P., Khaosaad, T., Toussaint, J.P., and Vierheilig, H. (2007). Flavonoids and strigolactones in root exudates as signals in symbiotic and pathogenic plant-fungus interactions. Molecules **12:** 1290–1306.

Stockinger, H., Walker, C., and Schüssler, A. (2009). '*Glomus intraradices* DAOM197198', a model fungus in arbuscular mycorrhiza research, is not *Glomus intraradices.* New Phytol. **183:** 1176–1187.

Stracke, S., Kistner, C., Yoshida, S., Mulder, L., Sato, S., Kaneko, T., Tabata, S., Sandal, N., Stougaard, J., Szczyglowski, K., and Parniske, M. (2002). A plant receptor-like kinase required for both bacterial and fungal symbiosis. Nature **417:** 959–962.

Strullu-Derrien, C., Selosse, M.A., Kenrick, P., and Martin, F.M. (2018). The origin and evolution of mycorrhizal symbioses: From palaeomycology to phylogenomics. New Phytol. **220:** 1012–1030.

Sukumar, P., Legué, V., Vayssières, A., Martin, F., Tuskan, G.A., and Kalluri, U.C. (2013). Involvement of auxin pathways in modulating root architecture during beneficial plant-microorganism interactions. Plant Cell Environ. **36:** 909–919.

Sun, J., et al. (2015). Activation of symbiosis signaling by arbuscular mycorrhizal fungi in legumes and rice. Plant Cell **27:** 823–838.

Tedersoo, L., and Smith, M.E. (2013). Lineages of ectomycorrhizal fungi revisited: Foraging strategies and novel lineages revealed by sequences from belowground. Fungal Biol. Rev. **27:** 83–99.

Tedersoo, L., May, T.W., and Smith, M.E. (2010). Ectomycorrhizal lifestyle in fungi: Global diversity, distribution, and evolution of phylogenetic lineages. Mycorrhiza **20:** 217–263.

Tisserant, E., et al. (2012). The transcriptome of the arbuscular mycorrhizal fungus *Glomus intraradices* (DAOM 197198) reveals functional tradeoffs in an obligate symbiont. New Phytol. **193:** 755–769.

Truchet, G., Roche, P., Lerouge, P., Vasse, J., Camut, S., De Billy, F., Promé, J.C., and Dénarié, J. (1991). Sulphated lipo-oligosaccharide signals of *Rhizobium meliloti* elicit root nodule organogenesis in alfalfa. Nature **351:** 670–673.

Tuskan, G.A., et al. (2006). The genome of black cottonwood, *Populus trichocarpa* (Torr. & Gray). Science **313:** 1596–1604.

Umehara, M., Hanada, A., Yoshida, S., Akiyama, K., Arite, T., Takeda-Kamiya, N., Magome, H., Kamiya, Y., Shirasu, K., Yoneyama, K., Kyozuka, J., and Yamaguchi, S. (2008). Inhibition of shoot branching by new terpenoid plant hormones. Nature **455:** 195–200.

van der Heijden, M.G.A., Martin, F.M., Selosse, M.-A., and Sanders, I.R. (2015). Mycorrhizal ecology and evolution: The past, the present, and the future. New Phytol. **205:** 1406–1423.

Vayssières, A., Pěnčík, A., Felten, J., Kohler, A., Ljung, K., Martin, F., and Legué, V. (2015). Development of the *Populus-Laccaria bicolor* ectomycorrhiza modifies root auxin metabolism, signalling and response. Plant Physiol. **169:** 890–902.

Venkateshwaran, M., Cosme, A., Han, L., Banba, M., Satyshur, K.A., Schleiff, E., Parniske, M., Imaizumi-Anraku, H., and Ané, J.-M. (2012). The recent evolution of a symbiotic ion channel in the legume family altered ion conductance and improved functionality in calcium signaling. Plant Cell **24:** 2528–2545.

Venkateshwaran, M., Volkening, J.D., Sussman, M.R., and Ané, J.M. (2013). Symbiosis and the social network of higher plants. Curr. Opin. Plant Biol. **16:** 118–127.

Venkateshwaran, M., Jayaraman, D., Chabaud, M., Genre, A., Balloon, A.J., Maeda, J., Forshey, K., den Os, D., Kwiecien, N.W., Coon, J.J., Barker, D.G., and Ané, J.-M. (2015). A role for the mevalonate pathway in early plant symbiotic signaling. Proc. Natl. Acad. Sci. USA **112:** 9781–9786.

Wang, B., and Qiu, Y.-L.L. (2006). Phylogenetic distribution and evolution of mycorrhizas in land plants. Mycorrhiza **16:** 299–363.

Yano, K., et al. (2008). CYCLOPS, a mediator of symbiotic intracellular accommodation. Proc. Natl. Acad. Sci. USA **105:** 20540–20545.

Yoneyama, K., Yoneyama, K., Takeuchi, Y., and Sekimoto, H. (2007). Phosphorus deficiency in red clover promotes exudation of orobanchol, the signal for mycorrhizal symbionts and germination stimulant for root parasites. Planta **225:** 1031–1038.

Yoshida, K., Ma, D., and Constabel, C.P. (2015). The MYB182 protein down-regulates proanthocyanidin and anthocyanin biosynthesis in poplar by repressing both structural and regulatory flavonoid genes. Plant Physiol. **167:** 693–710.

Zhang, X., Dong, W., Sun, J., Feng, F., Deng, Y., He, Z., Oldroyd, G.E.D., and Wang, E. (2015). The receptor kinase CERK1 has dual functions in symbiosis and immunity signalling. Plant J. **81:** 258–267.

Zhao, Y., Araki, S., Wu, J., Teramoto, T., Chang, Y.F., Nakano, M., Abdelfattah, A.S., Fujiwara, M., Ishihara, T., Nagai, T., and Campbell, R.E. (2011). An expanded palette of genetically encoded Ca^{2+} indicators. Science **333:** 1888–1891.